OGO 6 ION CONCENTRATION IRREGULARITY STUDIES

J. P. McClure
The University of Texas at Dallas
P. O. Box 30365
Dallas, Texas 75230

September 1973
Final Report for Contract NAS 5-23184

Prepared for

GODDARD SPACE FLIGHT CENTER
Greenbelt, Maryland 20771

Introduction. In this final report the research concerning ionospheric F-region irregularities under NASA contract NAS-5-23184 at The University of Texas at Dallas is described. Our results are based on in-situ measurements of the total ion concentration N_i made using the Ogo 6 satellite. The research objectives stated in the abstract of the proposal were "describing the data in ways appropriate for understanding the effect of the irregularities on radio propagation and for understanding the origin of the irregularities." Specifically the objectives included "determining the irregularity occurrence patterns and examining the power spectral intensity of the irregularities."

Many new and physically interesting morphological features were discovered in the data, as described below, but complete occurrence patterns, similar to those based on scintillation observations, were not obtained because of computer processing delays and overall time limitations. Since the data contained no obvious discrepancies with existing overall occurrence patterns, we concentrated on some of the unique morphological details of the data in areas where little or no previous information existed and where the new results would have obvious utility for understanding the irregularities themselves and related radio propagation effects. Perhaps the most interesting result of the research, one not specifically anticipated in our research objectives summarized above, was that we were able to suggest a mechanism which appears to explain successfully all of the observed features of

equatorial irregularities, including the at first glance paradoxical new data from Ogo 6 on the relationship between the presence of irregularities and Fe^+ ions in the equatorial ionosphere. The morphological results include the discovery of a minimum in $\Delta N_i/N_i$ at night in the region of the midlatitude trough in N_i. The poleward edge of the trough is almost always associated with the onset of soft auroral electron fluxes and large amplitude irregularities in N_i. When irregularities exist equatorward of the trough they tend to have a larger percentage (and absolute) amplitude than those in the trough. This minimum within the trough of $\Delta N_i/N_i$ may be related to the (unknown) mechanism which causes the N_i trough itself to develop. Finally, the large amplitude auroral irregularities which occur in the high latitude dayside ionosphere have been found to be intimately related to the so-called "dayside cusp" $\lesssim$ 300 eV electron fluxes, which can strongly interact with the atmosphere at F-region altitudes.

In the following sections we describe briefly our proposed mechanism for the generation of equatorial F-region irregularities and our morphological results in various latitude regions. A more detailed explanation of these results is given in the attachments, which consist of four scientific papers prepared in part with support from and in the time period of contract NAS-5-23184. Related results, published prior to the period of the present contract, are also discussed below for completeness. The subjects of the attached scientific papers are:

1) The cause of equatorial F-region irregularities (Hanson, McClure

and Sterling, 1973); 2) Morphological characteristics of F-region irregularities at low, middle and high latitudes (McClure and Hanson, 1973); 3) Spectral properties of these irregularities (Dyson, McClure and Hanson, 1973), and; 4) Detailed relationships between auroral irregularities and soft particle precipitation (Dyson and Winningham, 1973).

The cause of equatorial spread F. Instrumental problems were suspected when Ogo 6 data began indicating the presence in the nighttime equatorial F region of small concentrations (usually 5 to 500 cm^{-3}) of an ion roughly twice as heavy as the heaviest expected F-region ions (NO^+, O_2^+, N_2^+, all near 30 AMU). Such data were not returned from the satellite except at equatorial latitudes. The evidence soon became overwhelming that the unknown ion was Fe^+, and that in addition the presence of at least a detectable amount (our sensitivity limit for ions of mass >30 AMU was near 5 cm^{-3}) of Fe^+ is a necessary but not a sufficient condition for the generation of equatorial ionospheric irregularities. Such irregularities were observed without Fe^+ only 2.5% of the time, whereas Fe^+ was commonly observed without irregularities. Both this relation and indeed the very presence of Fe^+ above 400 km in the F region were very hard to believe in at first, even for ourselves. However at the present time meteoric ions have been independently detected in the equatorial F region by at least two other techniques (optically and via an ion mass spectrometer). Also, the source of these ions is understood (vertical electromagnetic drifts from the source region near 100 km altitude into the F region: the initial lifting from 100 km

is induced by vertical electric fields which can occur only within a few hundred km of the geomagnetic dip equator).

The latest result, obtained within this contract period, is that we believe we now know why trace amounts of Fe^+ ions are virtually always found on or near equatorial field tubes containing ionospheric irregularities. Time delay considerations clearly show it is not the irregularities which somehow transport the Fe^+ into the upper F region (this is incompatible with the above-mentioned evidence regarding Fe^+ as a necessary but not sufficient condition for equatorial irregularities). Hanson et al. (1973, attached) suggest that the basic cause of equatorial irregularities is electric fields generated in the ionosphere by zonal or meridional neutral winds acting on regions having structure in their field aligned Pedersen conductivity integrals. The conductivity structure, it is suggested, is caused by large "fingers" of long-lived metallic ions that randomly extend downward to ∿150 km, well below the normal nighttime F layer. The resulting plasma convection leads to large-scale (>10 km) irregularities and sets up gradients in the electric field and/or plasma pressure that drive other instability mechanisms to produce smaller-scale irregularities. The proposed mechanism requires a different neutral wind velocity above and below approximately 200 km for winds in the magnetic east-west direction; but, for winds in the magnetic meridion direction, such a velocity gradient is not required. We believe this mechanism may explain the enhanced occurrence probability for irregularities in the Atlantic zone seen in data from the Ogo 6 satellite, since zonal

winds have their largest magnetic meridional component in this sector. Also, since both the metallic ion distribution and the irregularities are believed to be approximately field aligned, the two should be strongly correlated in the upper F region, as observed in the Ogo 6 data.

In addition to being consistent with these two new Ogo 6 results on equatorial irregularities (the Atlantic maximum and the relation with Fe^+), the proposed mechanism is also consistent with radar observations of equatorial spread F (McClure and Woodman, Journal of Geophysical Research 77, 5617, 1972). These radar observations showed that the vertical drift velocity (or east-west electric field) in a wide region of well developed spread F was enhanced and turbulent, reaching positive and negative maximum values several times larger than the steady velocity of the undisturbed ionosphere and changing irregularly every few tens of km in altitude and every few minutes in time. We believe that such turbulent electric fields could be generated by the proposed mechanism.

However, there is another category of spread F observed at Jicamarca which has characteristics different from those described by McClure and Woodman. It occurs in thin layers on the bottomside of the F region, near the altitude where N_e reaches approximately 1% of its maximum value. It drifts with the background drift velocity of the undisturbed F region; i.e., it is not associated with enhanced and turbulent electric fields. We believe that this type of spread F may be associated with the large N_e gradients that normally exist in this part of the bottomside equatorial F region at night (Hanson et al., 1973).

The morphology of F-region irregularities. McClure and Hanson (1973, preprint attached) discussed some of the unique aspects of irregularity behavior as observed in the Ogo 6 data bank, concentrating on the actual N_i waveforms observed and the behavior of $\Delta N_i/N_i$ as a function of other possibly related geophysical phenomena observed using the same satellite. It was found, for example, that at night if midlatitude irregularities are present there is often a minimum in $\Delta N_i/N_i$ in the midlatitude trough region, and that in almost all cases the poleward edge of the nighttime trough is associated with the onset of soft auroral electron fluxes and large amplitude N_i irregularities, as mentioned in the introduction. Midlatitude irregularities are not correlated with the presence or absence of conjugate photoelectron fluxes.

Various distinct categories of irregularity waveforms are observed. Most irregularities have a "noiselike" waveform. This applies at all latitudes and local times. The other categories, present less than 10% of the time, are 1) quasi-sinusoidal waveforms, an equatorial phenomenon; 2) "ground glass" irregularities, having components only at wavelengths shorter than a few km, a midlatitude phenomenon; and 3) "breaking waves" or "sawtooth" irregularities, seen at all latitudes. The spectral properties of the irregularities are described in detail in the attached preprint by Dyson et al. (1973). The most common spectrum observed (that of the "noiselike" irregularities) was of the form $A = kS^n$, where A is the irregularity amplitude and S is the scale size or irregularity wave-

length. The spectrum was measured over the size range 70 m to 7 km, and the values of n obtained were close to one, the average value being .95. There were no significant variations in the spectral index n as a function of the rms irregularity amplitude over a 2.5 decade amplitude range (.1% to 25%). Examples of other types of spectra associated with the quasi-sinusoidal irregularities and with "ground glass" irregularities are also presented. These spectral results constitute a very crucial test that must be met by any detailed theory of F-region irregularities.

Dyson and Winningham (1973, preprint attached) made a morphological study using data relevant to high latitude phenomena and found that large amplitude F-region irregularities are intimately related to particle precipitation on the dayside of the auroral oval. Suggestions have often been made that precipitation might be responsible for the production of ionospheric irregularities in the auroral region. For example, Dyson (Journal of Geophysical Research, 74, 6291, 1969) showed that the occurrence of large amplitude auroral irregularities is similar to that of various auroral phenomena. However, no direct observations of a one-to-one relation between irregularities and particles had ever been documented prior to the work of Dyson and Winningham.

It was found that the equatorward edge of the "strong topside irregularity zone" (stiz) generally coincides with the equatorward edge of the $\lesssim$300 eV electron precipitation. The stiz usually extends beyond the poleward edge of the precipitation. This is presumably caused by magnetospheric convection transporting the irregularities poleward of the region of production.

The particles responsible for the F-region irregularities appear to be only those with energy $\lesssim$300 eV. No correlation was found between irregularities and particles having energy $\gtrsim$300 eV. This result is reasonable since only the lower energy particles interact strongly with the atmosphere at F-region heights. The conclusion reached was that the ionizing and heating effects of the particle precipitation could produce the irregularities, but other physical processes could also be important.

Summary and Conclusions. The research which was partially supported under NASA Contract NAS 5-23184 has provided a great deal of new information of fundamental importance in dealing with the practical problems of radio propagation through an ionosphere containing small scale inhomogenieties in N_i. We have provided a statistical description of the amplitude versus scale size spectrum of the irregularities showing that the irregularity amplitude is directly proportional to the scale size in almost all cases, independent of the location or the severity of the irregularities. This result is valuable in several areas, including theoretical modeling of ionospheric radio scintillation and attempts to understand the origin of the irregularities. Our other morphological results at high and low latitudes have clearly increased our understanding of irregularity occurrence patterns obtained from topside ionospheric sounding and from radio scintillation observations.

Finally, our observations of the detailed relationships between irregularities and other geophysically significant parameters have permitted us to outline some of the details of the source mechanisms for the

irregularities. For example a detailed relation was found, as might have been expected, between strong irregularities and the precipitation of soft electrons. A much more unexpected result was being able to postulate a reasonable mechanism which explains the very puzzling correlation between Fe^+ ions and irregularities in the equatorial F region. At the same time this mechanism appears to explain the origin of the irregularities themselves in a manner consistent with all the available observational data about them.

On the Cause of Equatorial Spread *F*

W. B. HANSON, J. P. MCCLURE, AND D. L. STERLING

University of Texas at Dallas, Dallas, Texas 75230

Summary. It is suggested that convective electric fields in the equatorial ionosphere are generated by neutral winds (either zonal or meridional) acting on regions having structure in their field aligned Pedersen conductivity integrals. The conductivity structure is presumed to be caused by long-lived metallic ions that have been concentrated irregularly below the *F* layer at altitudes where their collision and gyrofrequencies are comparable. The resulting plasma convection leads to large-scale (>10 km) irregularities and sets up gradients in the electric field and/or plasma pressure that drive other instability mechanisms to produce smaller-scale irregularities. The proposed mechanism requires a different velocity above and below approximately 200 km for winds in the magnetic east-west direction; but, for winds in the magnetic meridian direction, an altitude gradient is not required. This may help to explain the enhanced occurrence probability for irregularities in the Atlantic zone seen in data from the Ogo 6 satellite [*Hanson and Sanatani*, 1971], since zonal winds have their largest magnetic meridional component in this sector. Also, since both the metallic ion distribution and the irregularities are believed to be approximately field aligned, the two should be strongly correlated in the upper *F* region, as has been observed by Hanson and Sanatani.

Discussion. It was tentatively concluded after considerable deliberation that the presence of trace amounts of Fe^+ ions is an almost necessary condition for the formation of equatorial *F* region electron concentration irregularities based on unexpected data from the Ogo 6 satellite [*Hanson and Sanatani*, 1971]. However, since Fe^+ is often present without irregularities, it is clear that at least one other condition must also be met. These conclusions follow from the observation that structure was present without Fe^+ on only 2.5% of the equatorial passes examined, whereas Fe^+ was present without structure nearly one-fourth of the time.

The importance of the integrated Pedersen conductivity along magnetic field lines at *E* region altitudes Σ_{1E} in controlling the response of the equatorial *F* layer to east-west winds has been discussed by *Rishbeth* [1971]. He showed that, when Σ_{1E} is small compared with the *F* region integrated Pedersen conductivity Σ_{1F}, an induced polarization field is set up by the *F* region winds causing the *F* region plasma to drift in the east-west direction at nearly the *F* region neutral wind velocity even though at lower altitudes the neutral wind differs from that at higher altitudes. In the daytime, $\Sigma_{1E} \gg \Sigma_{1F}$, so that the *F* region plasma motions are governed by the *E* region dynamo electric field.

The point we wish to make is that at night even relatively small concentrations of ions N_i, if present in the region where their collision and gyrofrequencies (ν_i and ω_i) are nearly equal, may contribute substantially to the Pedersen integrals. Thus, if metallic ions are nonuniformly distributed in the region near 140 km, as they are observed to be at higher altitudes, the *F* region plasma magnetically connected to this region may tend to have a wide spectrum of drift velocities if the east-west neutral winds are different in the two altitude regions. Because of the incompressibility of the magnetic field, the ion drift velocities in the disturbed regions may assume vertical as well as east-west components. Also there will be shear regions near the boundaries of the disturbed zones where the more uniform plasma with lower Σ_{1E} conductivity flows around and past the field tubes partially shorted out by the metallic ions. It is possible that even if the Fe^+ region initially gave rise to a uniform high Σ_{1E} region it would become unstable because of the higher plasma flow veloc-

ity surrounding this region [*Völk and Haerendel*, 1971].

The conditions described above might well lead to layers of enhanced and turbulent electric fields in the F region (such as those observed by *McClure and Woodman* [1972]), and these turbulent fields could lead to large-scale (tens of km) irregular plasma convection and to smaller-scale irregularities in plasma concentration via one or more instability mechanisms. *Farley et al.* [1970] noted that most of the plasma instability mechanisms invoked to explain equatorial spread F, which could not be ruled out based on VHF radar data, require a gradient in either N_e or the electric field. Gradients in both these parameters would surely be established in the nighttime equatorial F region if, as we speculate, Fe^+ ions are nonuniformly distributed in the region between the E and the F layers.

There are substantial reasons to believe that there may be some validity to this view. *Hanson and Sanatani* [1971] reported that, on many satellite passes, Fe^+ and irregularities appear and disappear simultaneously as many as four or five times near the magnetic equator, whereas the ionosphere is smooth and contains no detectable Fe^+ between these segments. These observations are consistent with radar observations at Jicamarca [*Farley et al.*, 1970], where horizontal layers of irregularities are found to be vertically separated by regions without irregularities. Furthermore, layers of ionization have been observed at Arecibo near the region where $\nu_i \simeq \omega_i$ at night, and *Rowe and Gieraltowski* [1972] have interpreted these layers in terms of metallic ions that had been driven out of the F region by poleward winds.

Little information on the vertical or east-west horizontal structure of the Fe^+ ion distribution in the F region is available. It is believed that the source of these ions is near 100 km and that they are lifted to the F region by the (nonuniform) dynamo electric field, which is capable of causing patchiness in the resulting Fe^+ distribution as described by *Hanson et al.* [1972]. As the F region plasma moves downward below the F peak, the total ion concentration decreases because of recombination; thus the fractional abundance of Fe^+ increases in this region. If the Fe^+ is not removed rapidly to the region below 120 km, the steady flux out of the F region may also cause an increase in the absolute abundance of Fe^+ below the F peak. Thus the Fe^+ ions observed in the upper F region may provide only a tracer to the magnetic field tubes that are so populated, whereas the convective forces are exerted at much lower altitudes. Usually, deposition of the metallic ions in the bottomside F layer would take place at low tropical latitudes, because the Fe^+ ions are rarely observed as high as 30° dip latitude. The observations of *Rowe and Gieraltowski* [1972] followed a period of high magnetic activity, and these layers are normally not present at Arecibo. The Fe^+ ions should normally be observed only on field lines that cross the magnetic equator below approximately 1000 km, since the integral of the upward daytime plasma velocity observed with the Jicamarca radar [*Woodman*, 1970] is typically of the order of 1000 km between the morning and the evening reversal of this velocity.

Rishbeth's [1971] discussion of the influence of the east-west neutral wind on the F region plasma motion can be straightforwardly extended to account for north-south wind effects by including the factor $\sin I$, where I is the magnetic dip angle, in the Pedersen integrand. In this case a uniform north-south wind acting on a symmetric plasma distribution would not produce inward or outward convection because, although the induced polarization field generated in the northern hemisphere would tend to convect the plasma inward, that generated in the southern hemisphere would tend to convect it outward, and the high conductivity along the geomagnetic field lines would mutually short out these induced polarization fields. However, if the Pedersen integrals (including $\sin I$) of the two hemispheres were unequal, the polarization electric field set up in the hemisphere with the largest integral would dominate, and inward or outward plasma convection would occur. Here again, horizontal structure in N_e in the $\nu_i \simeq \omega_i$ region could lead to turbulent F region convection, but, in this case, no vertical gradients in the neutral winds are required.

We mention this because one salient feature of the Ogo 6 data of *Hanson and Sanatani* [1971] remains unexplained, namely, that of the very high incidence of equatorial irregularities in the Atlantic longitude sector. The $\sin I$ weighting factor that applies for magnetic

meridional winds gives an even greater relative emphasis in the Pedersen integrals to the ionization near the ends of the magnetic tubes. Thus, if the irregularity production mechanism we are proposing is correct, then the sensitivity should be greater to magnetic meridional winds than to those in the magnetic east-west direction. Because the equatorial magnetic declination is largest in the Atlantic region, purely zonal (geographic) winds produce the greatest magnetic meridional wind components there. Thus, if zonal winds are normally large compared with meridional (geographic) winds, this might explain the higher occurrence of irregularities in the Atlantic region. Even if it should turn out that this is not the correct explanation of the 'Atlantic enhancement' of irregularities, it is clear that either meridional or zonal winds (or both) could set up the irregular electric fields we have been discussing.

Balsley et al. [1972] have recently reinvoked the Rayleigh-Taylor instability to explain equatorial irregularities, but their version of this mechanism has two serious difficulties. It does not explain the connection with Fe^+ ions, and it cannot explain the vertical layers of irregularities that are observed using both the Ogo 6 satellite and the Jicamarca radar. It may be that the Rayleigh-Taylor mechanism, originally applied to this problem by *Dungey* [1956], or the gradient drift instability [*Prakash et al.*, 1971; *Martyn*, 1953], is important in producing smaller-scale irregularities once the initial turbulent convection has begun owing to the 'seeding' presence of the metallic ions.

We do not claim that all equatorial spread F is caused by the presence of Fe^+ ions. For example, a thin layer of weak spread F is often present at the lower edge of the F region when this edge is above a certain altitude [*Farley et al.*, 1970]. Ogo 6 did not explore the pertinent altitude region, but, when other satellites do, it may turn out that there is little or no relationship between Fe^+ ions and this spread F subclass, which occurs in a region where large N_e gradients normally exist as a result of ordinary chemical processes. Even here, however, unusually large gradients occasionally occur [*Hanson and Sanatani*, 1973], presumably because of convection effects.

Since few radar, rocket, or satellite measurements of Fe^+ (or even of N_e) have been made in the valley between the E and the F layers at equatorial latitudes, it is impossible to verify these speculations at this time. Ionosondes do not have the requisite sensitivity to do this, and, even if they did, the lower E layer might well shield the higher layer. It is a clear prediction of the theory and observations discussed by *Hanson et al.* [1972], however, that metallic ions should often be present in the normal valley between the E and the F layers. We have now predicted that this will be the case in at least one hemisphere when F region irregularities are present (north-south winds may drive most of the metallic ions to one hemisphere or the other). The atmosphere Explorer satellites will begin to probe the pertinent regions in 1974 and will have the necessary instrumentation (in cooperation with the Jicamarca radar) to examine the validity of these assertions.

Acknowledgments. This work was supported by NASA contract NAS 5-9311, NSF grant GA 31318, and by NAA grants 44-004-029 and 44-004-001.

REFERENCES

Balsley, B. B., G. Haerendel, and R. A. Greenwald, Equatorial spread F: Recent observations and a new interpretation, *J. Geophys. Res.*, *77*, 5625, 1972.

Dungey, J. W., Convective diffusion in the equatorial F region, *J. Atmos. Terr. Phys.*, *9*, 304, 1956.

Farley, D. T., B. B. Balsley, R. F. Woodman, and J. P. McClure, Equatorial spread F: Implications of VHF radar observations, *J. Geophys. Res.*, *75*, 7199, 1970.

Hanson, W. B., and S. Sanatani, Relationship between Fe^+ ions and equatorial spread F, *J. Geophys. Res.*, *76*, 7761, 1971.

Hanson, W. B., and S. Sanatani, Large N_e gradients below the equatorial F peak, *J. Geophys. Res.*, *78*, 1167, 1973.

Hanson, W. B., D. L. Sterling, and R. F. Woodman, Source and identification of heavy ions in the equatorial F layer, *J. Geophys. Res.*, *77*, 5530, 1972.

Martyn, D. F., Electric currents in the ionosphere, 3, Ionization drift due to winds and electric fields, *Phil. Trans. Roy. Soc. London Ser. A*, *246*, 303, 1953.

McClure, J. P., and R. F. Woodman, Radar observations of equatorial spread F in a region of electrostatic turbulence, *J. Geophys. Res.*, *77*, 5617, 1972.

Prakash, S., S. P. Gupta, and B. H. Subbaraya, Origin of irregularities in the E region, *Nature Phys. Sci.*, *130*, 170, 1971.

Rishbeth, H., Polarization fields produced by winds in the equatorial *F* region, *Planet. Space Sci., 19,* 357, 1971.

Rowe, J. F., Jr., and G. F. Gieraltowski, The formation and motion of nighttime sporadic *E* layers at Arecibo (abstract), *Eos Trans. AGU, 53,* 1077, 1972.

Völk, H. J., and G. Haerendel, Striations in ion clouds, *J. Geophys. Res., 76,* 4541, 1971.

Woodman, R. F., Vertical drift velocities and east-west electric fields at the magnetic equator, *J. Geophys. Res., 75,* 6249, 1970.

(Received January 18, 1973;
accepted January 29, 1973.)

Communicated by G. C. Reid.

A Catalog of Ionospheric F-Region Irregularity Behavior Based on Ogo 6 Retarding Potential Analyzer Data

J. P. McClure
and
W. B. Hanson
The University of Texas at Dallas
Dallas, Texas 75230

Accepted by the
Journal of Geophysical Research
June 1973

ABSTRACT

The OGO 6 Retarding Potential Analyser was used ∿ 50% of the time to measure the total ion concentration N_i along the satellite path. In this paper we catalog the waveforms of the ionospheric F-region irregularities observed and discuss their morphological behavior. The middle and low latitude ionosphere is usually remarkable smooth, to within at least 0.1% in $\Delta N/N$, even at night, if we ignore wavelengths greater than 100 km. Transitions from a smooth to an irregular ionosphere in several different latitude regions are presented and discussed. Transitions may be either abrupt or gradual. The poleward edge of the nighttime midlatitude trough is almost always associated with the onset of soft auroral electron fluxes and large amplitude auroral irregularities in N_i. If midlatitude irregularities are also present on a given pass there is often a minimum in $\Delta N/N$ in the trough region. Examples of low latitude irregularities are presented. These irregularities can have very large amplitudes, comparable to the largest auroral $\Delta N/N$ values. Since, ionospheric scintillation depends on ΔN and not $\Delta N/N$, one would therefore expect stronger scintillation at low than at high latitudes, as is observed, since equatorial N_i values are generally larger than those at high latitudes. The above morphological characteristics apply to the typical "noiselike" irregularity waveforms, whose spectral properties appear to be relatively constant, independent of e.g. latitude, local time or the RMS amplitude of $\Delta N/N$. In addition to the noiselike irregularities we catalog examples of other irregularity categories such as sinusoidal waveforms, an equatorial phenomonon; "ground glass" irregularities, mainly observed at midlatitudes; and "breaking waves," seen at all latitudes.

Introduction. A large amount of new information about F-region irregularities has been obtained from the Retarding Potential Analyzer (RPA) on the Ogo 6 satellite (perigee ∿400 km; apogee ∿1100 km; orbital inclination ∿82°). The instrument has been described in detail by Hanson et al. (1970). Briefly, the RPA was programmed to measure the total ion concentration $N_i(s)$ along the satellite path for 50% of the time, with the remainder of the time being devoted to measuring the ion temperature, ion composition, and other plasma parameters. In this paper we present and discuss some of the observed F-region irregularity waveforms. Ogo 6 has provided the first such detailed measurements. Earlier in-situ observations of F-region irregularities, made with the Alouette II ionosonde and Langmuir probe, have been used for morphological studies (Dyson, 1969; 1971), but the spatial and amplitude resolution of Dyson's data was inadequate to permit the detailed description of the actual ionospheric waveforms that is presented here.

The most common type of structure is a noiselike N_i fluctuation having a power spectral intensity which appears to be approximated by a power law with an exponent of the order of two. We present several examples of these typical ionospheric irregularities and discuss briefly their spectral properties and their occurrence patterns. We also show examples of several less common but very distinctive ionospheric irregularity waveforms, e.g., equatorial sinusoidal structure, a "ground glass"

category having no spectral power for scale sizes larger than a few hundred meters, and "breaking waves" resembling ocean waves about to break on a beach.

Instrumental operation. The instrument was used as a conventional RPA half the time and as an "irregularity detector" half the time. Each half cycle could be set to be either approximately 5 seconds or 20 seconds (roughly 40 or 160 km of orbital pathlength). In the conventional RPA half cycle we obtain the usual i-v curve, from which the ion temperature, composition, and under favorable conditions (significant concentrations of appropriate ions), the "ram" velocity v_r of the ions in the satellite frame of reference are inferred. In the "irregularity mode" none of the ions intercepted are retarded and hence the electrometer output is proportional to the product $N_i v_r$, where N_i is the total ion concentration. In this mode the electrometer output is connected to a difference amplifier (gain = 50) resulting in a variable sensitivity limit of between .03 and .01%, depending on the initial electrometer voltage (Hanson et al., 1970). The 50x amplifier saturates at a variable percentage value of $\Delta N_i/N_i$, usually between $\pm 1\%$ and $\pm 3.5\%$, again depending on the electrometer voltage at the start of the irregularity mode. The outputs of both the electrometer and the difference amplifier are telemetered during the irregularity mode.

The midlatitude scintillation boundary. In Figure 1 we show an example of the equatorward boundary of the high latitude scintillation region. This boundary has been studied via ground observations of satellite

scintillation, e.g. by Yeh and Swenson, 1964, and by Aarons et al., 1969. It was near invariant latitude $\Lambda \sim 58°$ for this example, obtained at 2215 hrs LT over the northern U. S. on November 20, 1969, a quiet day. The solid line is the difference amplifier output (left hand scale) and the dots are the electrometer output (right hand scale). The dots are spaced ~1.1 km apart and the data values for the solid line have approximately one-third of this spacing. In plotting, the line and the dots are normalized to 0.0 and 1.0, respectively, at the start of each data segment. The difference amplifier is seen to saturate when the percentage fluctuation $\Delta N_i/N_i$ reaches ~1% to 2% (cf. Λ = 57.7°, 59.5°, 60.1°, 60.6°, and 61.1).

The Ogo 6 results show that the scintillation boundary is usually quite gradual, as in the example shown here, although it can occasionally be extremely abrupt. This same behavior has been noted previously using other techniques. For example, McClure (1964) found that only on special occasions was it possible to determine the height of the scintillation producing irregularities by triangulation on the abrupt edge of an irregularity region; usually the boundary was more gradual and it was necessary to triangulate using the individual irregularities in the ground diffraction pattern in order to determine the height of the ionospheric irregularities responsible for the pattern.

Further discussion of irregularity boundaries. Figure 2 shows part of one orbit of Ogo 6 RPA data illustrating typical variations of the RMS value of Σ ($=\Delta N/N$) and some of the typical relationships between Σ and other parameters derived from the RPA. For clarity only Σ values >0.5% are shown, although our threshold for Σ is much lower (.01 to .03%). The center panel of the figure gives the flux of electrons of energy >10 ev, and the total ion concentration is plotted in the lower panel. Invariant latitude Λ, magnetic dipole local time and satellite altitude are given in the lower scales. The figure shows both a gradual equatorward boundary of the midlatitude irregularity region (in the northern hemisphere) and an abrupt boundary of this region (in the southern hemisphere). Stuart (1972) presents a statistical study based on satellite scintillation data of the abruptness and other details of midlatitude boundaries.

The two regions of equatorial irregularities near $\Lambda = \pm 20°$ latitude in in Figure 2 have abrupt boundaries, but equatorial boundaries can also be gradual, as we shall see below. These particular irregularity boundaries coincide very closely with the boundaries of the only two patches of Fe^+ ions observed on this orbit.

The electron flux is smoothly varying below 65° N and quite irregular above 65°N. No fluxes were observed in the southern hemisphere to 45°S, and no RPA flux data are available beyond 45°S. Conjugate photoelectrons are responsible for the smoothly varying flux between 55 and 65°N; the lower latitude limit of these fluxes is reached when the conjugate ionosphere is no longer sunlit, and we observe that this latitude depends of course on longitude, season, local time, etc. The irregular fluxes above 65°N are caused by auroral electrons (Winningham et al., 1973). The presence

or absence of midlatitude irregularities does not seem to be related to the presence or absence of conjugate photoelectrons.

In the example shown in Figure 2, the "midlatitude trough" in N_i (Muldrew, 1965; Sharp, 1966), centered near 65°N, is roughly rectangular in shape. Other Ogo 6 data show that it can take on a variety of other shapes as well as other widths and depths. The high latitude edge of the nightside trough is usually very steep and is almost always associated with the onset of soft auroral electron fluxes and enhanced values of Σ. Usually Σ reaches a maximum value of the order of 10 to 20% in the nighttime auroral zone and tends to decrease somewhat inside the polar cap, as it does in the example shown here. However, on some occasions Σ may reach very small values (< 1%) inside the polar cap, as illustrated in Figure 10 below.

When there are irregularities in the midlatitude ionosphere, our data often show that there is a minimum in $\Delta N/N$ in the trough region. An extreme example of such a minimum appears just below $\Lambda = 65°$ in Figure 2. The existence of such minima leads us to speculate that they may be a result of some of the same physical processes responsible for the trough. Since both N and $\Delta N/N$ tend to be smaller in the trough region than in higher or lower latitudes, there should be a pronounced minimum in ionospheric scintillation in that region.

Large amplitude equatorial irregularities. Auroral irregularities usually have a larger percentage value of $\Delta N/N$ than those found at any other latitude, but near the geomagnetic equator $\Delta N/N$ is occasionally as large as the largest auroral values. An example of such equatorial irregularities is shown in Figure 3. The difference amplifier was saturated; its output is not shown. The 1.1 km resolution of the electrometer was not adequate to resolve the irregularities, but it is clear that N_i changed by up to nearly a factor of 2 between measurements in some cases. Even larger amplitude structure than shown here is observed, but the data is often difficult to interpret because the sensitivity of the electrometer automatically changes by a factor of $(10)^{1/2}$ when its output exceeds predetermined upper and lower bounds.

These large amplitude equatorial irregularities are probably associated with those responsible for the unexpected ionospheric scintillation which has recently been observed at frequencies up to 6 GHz (Christiansen, 1971; Sessions, 1972; Taur, 1973). Microwave scintillation also occurs at high latitudes (Pope and Fritz, 1970), but equatorial scintillation is roughly an order of magnitude stronger. This fact can be easily understood based on the Ogo 6 results. The scintillation index is proportional to the absolute value of ΔN and to the thickness of the irregularity region (Yeh, 1962). Since $\Delta N/N$ reaches comparable percentage values at both high and low latitudes, and since both N_{max} and the "thickness" of the ionosphere are much greater near the equator, and since it is known that irregularities often extend through the entire equatorial F region (McClure et al., 1970), a strong enhancement of equatorial over auroral scintillation would be expected.

Equatorial microwave scintillation reaches a maximum in "Atlantic" longitudes (Christiansen, 1970; Taur, 1973). This fact can also be

understood based on Ogo 6 data. F-region equatorial irregularity occurrence reaches a maximum in those same longitudes (Hanson and Sanatani, 1971). A possible theoretical explanation of this observation has been advanced by Hanson et al. (1973).

The fluctuation spectrum of typical F-region irregularities. All but a small fraction of the F-region structure is qualitatively similar to that shown in Figure 1. Perhaps 99% of the structure we observe falls into this "noiselike" category. Preliminary studies show that the power spectral intensity of such irregularities increases approximately as the square of their scale size; i.e. $\Delta N/N$ is approximately proportional to the irregularity scale size. Thus the actual spatial gradients of N are approximately independent of scale size. Further studies of the spectral and other statistical properties of the observed irregularity waveforms are presently in progress and will be reported later.

The spectral behavior of the irregularities places constraints on the possible irregularity production mechanisms. Power law spectra such as those it appears we observe are consistent with some form of turbulence as a possible production mechanism. Electrostatic turbulence has already been advanced as a possible source of equatorial irregularities by McClure and Woodman (1972), who observed enhanced and turbulent plasma velocities (electric fields) in a region of equatorial spread F. Hanson et al. (1973) have postulated a mechanism involving neutral winds and meteoric ions that would result in electrostatic turbulence in the equatorial F region.

The lower edge of the equatorial F region. In Figure 4 we show data from a pass where N_i dropped from near 10^6 to near 10^3 cm^{-3} in less than 63 km (~8 sec) along the satellite path, remained small and relatively constant for 31 km, during which time one perfect RPA i-v curve was obtained, and then increased to near its original value in approximately 86 km. The ion temperature both in the F layer and in the "hole" was near 1000°K and relatively constant. The ion composition in the F layer was predominantly O^+, with a small and slowly varying ion concentration of mass 30 $\pm$2 AMU and a few patches of Fe^+ ions, as shown in the figure. Inside the "hole" there was no detectable Fe^+ (< 8 cm^{-3}), little O^+ (approximately 100 cm^{-3}), and nearly 10^3 molecular ions/cm^3, which is approximately 20 times the molecular ion concentration found outside (see the dashed line in the figure, which for clarity was not extended upwards to include the one measurement obtained inside the "hole.")

Other examples of such decreases in N_i, though considerably larger in geographic extent, were presented by Hanson and Sanatani (1973) who suggested that these "holes" are associated with the steep bottomside of the F_2 layer. Typically the ion composition is vastly different inside and outside the "holes," but these composition changes have no set pattern. For example, Fe^+ ions may either be enhanced or, as in the present example, depleted. Molecular ions are usually enhanced, but the amount of the enhancement is highly variable. We believe this indicates that the field tubes crossed by the satellite while it is inside the depleted or "hole" region originally crossed the equator at much lower altitudes and were convected upwards by large scale irregular electric fields. These large bite-outs of N_i are invariably centered on the minimum L value or

magnetic apex latitude (VanZandt et al., 1972) crossed by the satellite, rather than on the dip equator, consistent with the above interpretation.

The location of two patches of small scale irregularities is shown in Figure 4. The boundaries of these patches coincide with the boundaries of the Fe^+ patches, as is often the case for equatorial irregularities (Hanson and Sanatani, 1970). The N_i curve has a large fluctuation near +12° dip latitude, the location of one of the patches of small scale irregularities. This large scale fluctuation was probably caused by large scale convective motions associated with the patch of small scale irregularities.

Sinusoidal waveforms. Figures 5 and 6 show nearly monochromatic irregularity waveforms. Such structure, which is usually observed only at low latitudes, is called sinusoidal to distinguish it from the more frequent stochastic spectra. In Figure 5 the sinusoids have a peak-to-peak amplitude of ∿5% and a wavelength of ∿13 km. In Figure 6 we show a set of i-v curves showing sinusoidal structure of ∿50% amplitude and ∿3 km wavelength. The structure is seen both in the total saturation current (mainly O^+) for retarding potentials $\phi < 6$ v and in the Fe^+ current (Hanson and Sanatani, 1970), which is the only current remaining for $\phi > 12$ v. The amplitude of these sinusoids is among the largest we have ever observed; intermediate amplitudes down to <.1%, near our threshold of sensitivity, have also been observed. Sinusoidal wavelengths usually lie between 1 and 20 km.

Occasionally sinusoids of small but gradually increasing amplitude are observed as the satellite approaches a region of equatorial irregularities. Figure 7 shows two such events observed on two adjacent orbits. Prior to

the start of the data shown there were no detectable irregularities. For each of the orbits (labeled A and B in the figure) there is a gradual increase in the amplitude of the sinusoidal irregularities and the Fe^+ concentration, indicated by the lower left-hand portion of the i-v curves shown in the odd-numbered panels. The ionosphere continued to be irregular for some distance after the data segments shown. These events are relatively rare, but they have been seen on several other occasions.

Ground glass irregularities. Occasionally we see an irregularity subclass which we have tentatively labeled "ground glass" because, in contrast with the more common noiselike or stochastic irregularities we observe, the amplitude of this subclass always remains small (<1%) and almost all of the spectral power is contained in the smaller scale sizes. An example of this subclass is shown in Figure 8. This behavior is often observed near the mid-latitude scintillation boundary and it is usually characterized by a peak-to-peak amplitude of less than one percent.

Breaking wave irregularities. In Figure 9 we show an example of a subclass of irregularity waveforms which we have tentatively labeled "breaking waves" because of their resemblance to ocean waves about to break on a beach. These waveforms have been seen at all latitudes. The crest to trough amplitude for the example shown is of the order of 10%, although these waveforms usually have smaller amplitudes. The waves shown in Figure 9 and others not shown from the same equatorial pass change their sense at the time the satellite crosses the geomagnetic equator. This reversal phenomenon has been observed only once.

Regions of smooth and irregular ionization inside the polar cap. Figure 10 shows 4 consecutive segments of N_i data, labeled 1 through 4 in a slightly different format than shown before. Here the satellite

potential is large and negative, so that ions are not prevented from reaching the collector even during the voltage sweep time period. During this time the difference amplifier is AC coupled to the electrometer output with a gain of approximately 10 and a passband extending from 20 to 80 Hz. In the format shown the un-normalized electrometer output is plotted, together with the difference amplifier output whose AC ground is located at the center of the voltage scale. The figure shows a series of isolated regions of moderately strong irregularities separated by relatively quiet regions. The RMS value of $\Delta N/N$ is of the order of several percent in the disturbed patches and a few tenths of a percent or lower in the less disturbed regions. Although high latitude irregularities usually extend across the entire polar cap with moderate to high amplitude as mentioned above, many high latitude examples exist having gaps such as those of Figure 10.

Discussion The RPA on Ogo 6 has provided a wealth of in-situ data that reveals the nature of ionosphere irregularities in N_i above 400 km. Except for the high latitude regions the ionosphere is usually observed to be very smooth in the daytime, but considerable structure is observed at night, particularly near the equator and at Atlantic longitudes. While most of the irregularities observed appear to be stochastic in nature, many nearly monochromatic waveforms are observed near the equator. Several different theories of the origin of ionospheric irregularities are beginning to emerge and we have presented data here which we hope will provide useful tests for these concepts.

While the emphasis in this paper has been on irregularities in N_i it should be kept in mind that at midlatitudes the ionosphere is usually

remarkably smooth, certainly to within 0.1 percent, even at night, if we ignore wavelengths greater than several hundred kilometers.

A question that seems pertinent for the equatorial region in this regard is how the massive irregularity structure observed there at night can heal so rapidly that it is not seen in the daytime. It is true that photoionization and recombination will tend to smooth N_i in sunlight, but spread-F and scintillation studies show that the irregularities tend to disappear before sunrise. It seems possible that the downward $\overline{E} \times \overline{B}$ motion of the plasma observed at night might transport most of the disturbed plasma regions to low altitudes, where recombination is high, and in this manner remove the large irregularities. Or perhaps there are stabilizing mechanisms, in contrast to instability mechanisms, that actively tend to force uniformity on the N_i concentration (i.e., the crossed field instability mechanism with reversed ΔN_i). This question of the disappearance mechanism, as well as the one concerning irregularity formation, deserves attention.

Acknowledgments: We acknowledge helpful discussions with Dr. P. L. Dyson. This work was supported in part by NSF Grant GA-31318, NASA Grant NGL-44-004-001, and NASA Contracts NAS 5-9311 and NAS 5-23184. Support was also received from The University of Texas at Dallas Research Fund.

References

Aarons, J., J. P. Mullen and H. E. Whitney, The scintillation boundary J. Geophys. Res., 74, 884, 1969

Christiansen, Ross M., Preliminary report of S-band propagation disturbance during ALSEP mission support, NASA Report X-861-71-239, June 1971

Dyson, P. L., Direct measurement of the size and amplitude of irregularities in the topside ionosphere, J. Geophys. Res., 74, 6291, 1969

Dyson, P. L., On the significance of electrostatic probe observations of electron density irregularities, J. Geophys. Res., 76, 4689, 1971

Farley, D. T., B. B. Balsley, R. F. Woodman and J. P. McClure, Equatorial spread F: Implications of VHF radar observations, J. Geophys. Res., 75, 7199, 1970

Hanson, W. B., S. Sanatani, D. Zuccaro, and T. W. Flowerday, Plasma measurements with the retarding potential analyzer on Ogo 6, J. Geophys. Res., 75, 5483, 1970

Hanson, W. B., and S. Sanatani, Meteoric ions above the F_2 peak, J. Geophys. Res., 75, 5503, 1970

Hanson, W. B., and S. Sanatani, Relationship between Fe^+ ions and equatorial spread F, J. Geophys. Res., 76, 7761, 1971

Hanson, W. B., J. P. McClure, and D. L. Sterling, On the cause of equatorial spread F, accepted for publication in J. Geophys. Res., 1973

Hanson, W. B., and S. Sanatani, Large N_i gradients below the equatorial F peak, J. Geophys. Res., 78, 1167, 1973

McClure, J. P., The height of scintillation-producing ionospheric irregularities in temperate latitudes, J. Geophys. Res., 69, 2775, 1964

McClure, J. P., D. T. Farley, Jr., and R. Cohen, Ionospheric electron concentration measurements at the magnetic equator, 1964-1966, ESSA Tech. Rep. ERL 186-L 4, Environ. Sci. Serv. Admin., ESSA Res. Lab., Boulder, Colo., 1970

McClure, J. P., and R. F. Woodman, Radar observations of equatorial spread F in a region of electrostatic turbulence, J. Geophys. Res., 77, 5617, 1972

Muldrew, D. B., F-layer ionization troughs deduced from Alouette data, J. Geophys. Res., 70, 2635, 1965

Pope, J. H., and R. B. Fritz, Observations of simultaneous scintillation on VHF and S-band satellite transmissions at high latitudes, NOAA Tech. Rep. ERL 207-OD 6, Boulder, Colo., 1970

Sessions, W. B., Amplitude fading of simultaneous transionospheric L-band and VHF signals received at the geomagnetic equator, GSFC x-810-72-282, June 1972

Sharp, G. W., Midlatitude trough in the night ionosphere, J. Geophys. Res., 71, 1345, 1966

Stuart, G. F., Characteristics of the abrupt scintillation boundary, J. Atmos. Terr. Phys. 34, 1455, 1972

Taur, R. R., Ionospheric scintillation at 4 and 6 GHz, COMSAT Lab Tech. Memorandum CL-43-72, 1972

VanZandt, T. E., W. L. Clark, and J. M. Warnock, Magnetic apex coordination: A magnetic coordinate system for the ionospheric F_2 layer, J. Geophys. Res., 77, 2406, 1972

Winningham, J. D., S.-I. Akasofu, F. Yasuhara and W. J. Heikkila, Simultaneous observations of auroras from the South Pole Station and of precipitating electrons by ISIS-1, accepted for publication, J. Geophys. Res., 1973

Yeh, K. C., Propagation of spherical waves through an ionosphere containing anisotropic irregularities, J. Res. NBS 66D (Radio Prop.), No. 5, 621, 1962

Yeh, K. C. and G. W. Swenson, Jr., F-region irregularities studied by scintillation of signals from satellites, Radio Sci., 68, 881, 1964

Figure Captions

Fig. 1 The midlatitude scintillation boundary. Ion concentration variations determined from the electrometer (dots, right hand scale) and duct amplifier (solid line, left hand scale). (1969 day 324, orbit 2422, 2215 hrs LT.)

Fig. 2 The midlatitude N_i trough. This figure illustrates typical relationships between N_i, the flux of electrons of energy >10 ev, and the RMS amplitude of the ionospheric irregularities. (1970 day 23, orbit 3347.)

Fig. 3 Large amplitude equatorial irregularities. Such irregularities are particularly common in "Atlantic" longitudes, from roughly -70° to +30°. This sample was obtained over Brazil at 406 km altitude, 0° dipole latitude, -51° longitude, and 2117 hrs LT. (1969 day 325, orbit 2434.)

Fig. 4 Large N_i gradients beneath the equatorial F region. In this example N_i dropped by 3 orders of magnitude in <63 km along the satellite path, then recovered in ∿86 km. The boundaries of the patches of ionospheric irregularities ($\Sigma = \Delta N_i/N_i$) coincide with the boundaries of the patches of $56^+(Fe^+)$ ions. (1969 day 322, orbit 2404, ∿400 km altitude, -22° longitude, and ∿2105 hrs LT.)

Fig. 5 Nearly monochromatic waveforms, an equatorial phenomenon. (1969 day 324, orbit 2420, -10° dipole latitude, -62° longitude, 431 km altitude, 2116 hrs LT.)

Fig. 6 Large amplitude sinusoidal waveforms. The dip latitudes are indicated on these six RPA i-v curves which have ∿50% modulation of the total saturation current (mainly O^+) to the right of 6 volts and a similar modulation of the Fe^+ current to the left of 12 volts. (1969 day 323, orbit 2410, ∿400 km altitude, -170° longitude, 2148 hrs LT.)

Fig. 7 Gradual onset of sinusoidal irregularities on two adjacent Ogo 6 orbits. The Fe^+ concentration, indicated by the lower left portions of the i-v curves, also gradually increases. Orbits A and B (7693 and 7694) were near -126° and -151° longitude on 1970 day 322, at ∿455 km altitude and 2230 hrs LT. Prior to sweeps 1A and 1B (-15.0° and -12.4° dip latitude) there was little or no detectable structure or Fe^+; after sweeps 12A and 12B (-11.9° and -9.2° dip latitude) the then existing structure continued for some distance.

Fig. 8 "Ground glass" irregularities. (1969 day 322, orbit 2395, 503 km altitude, 60° dipole latitude, -122° longitude, 2230 hrs LT.)

Fig. 9 "Breaking wave" ionospheric irregularities. The dip latitude is shown on the figure. (1970 day 324, near 455 km altitude, -77° longitude, and 2207 hrs LT.)

Fig. 10 Bursts of auroral F-region irregularities. Four consecutive segments (#1 through #4) of Ogo 6 RPA telemetry output. For this example the electrometer telemetry level (proportional to $N_i v_r$) is always >128, and the difference amplifier, output centered at 128, is AC coupled with a gain near 10 and a 20- to 60-Hz passband. (1970 day 154, 492 km altitude, -68° longitude, 71° latitude.)

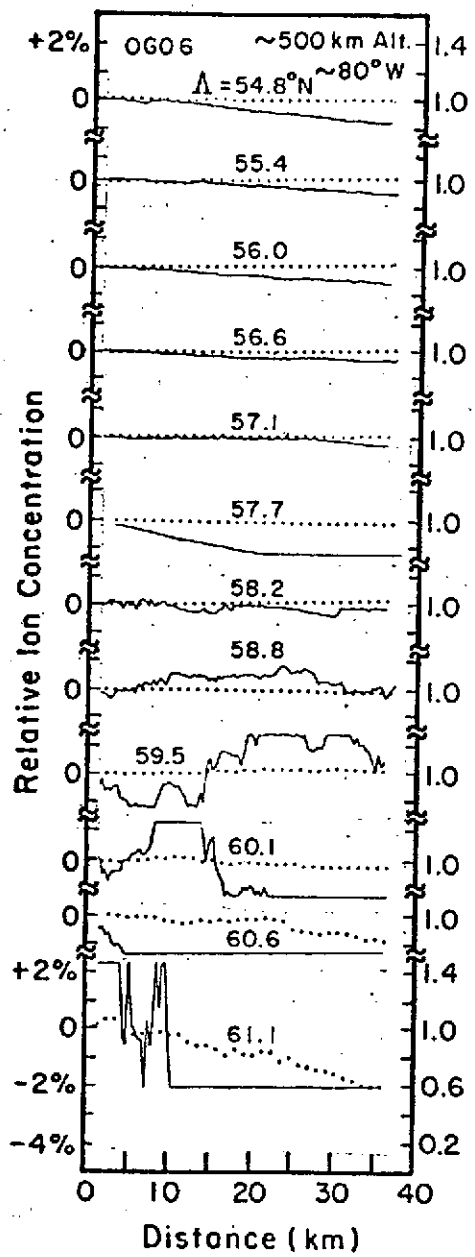

Fig. 1

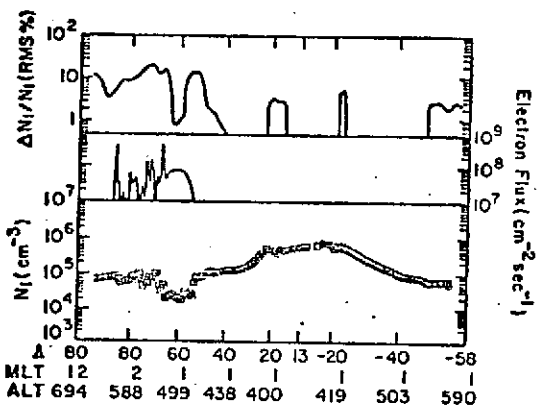

Fig. 2

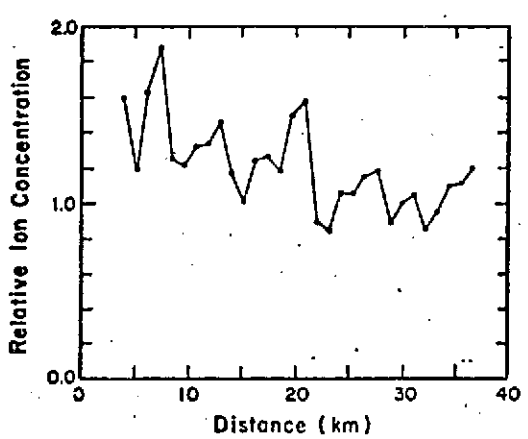

Fig. 3

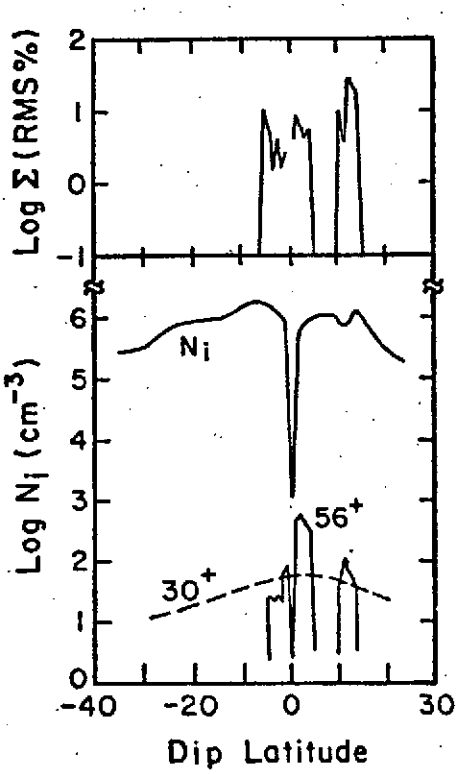

Fig. 4

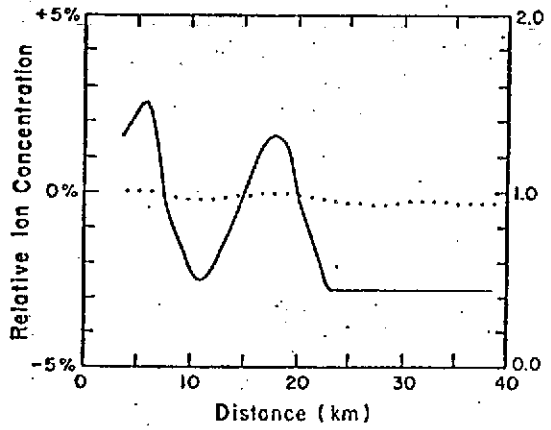

Fig. 5

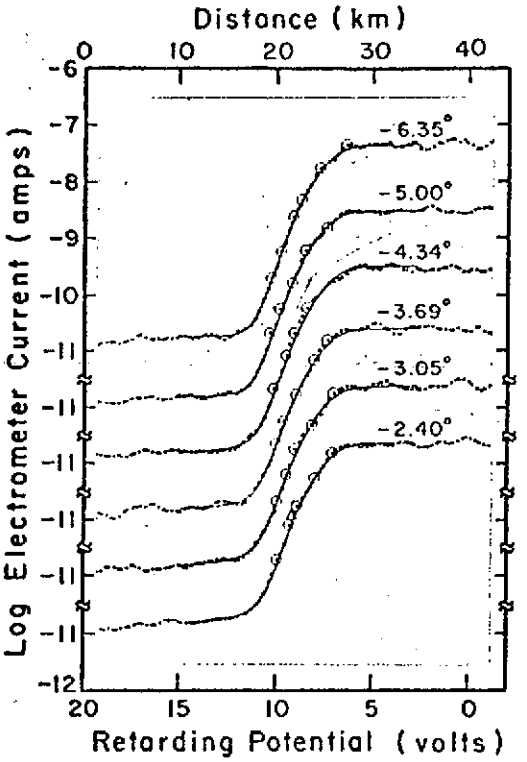

Fig. 6

Fig. 7 (See next page.)

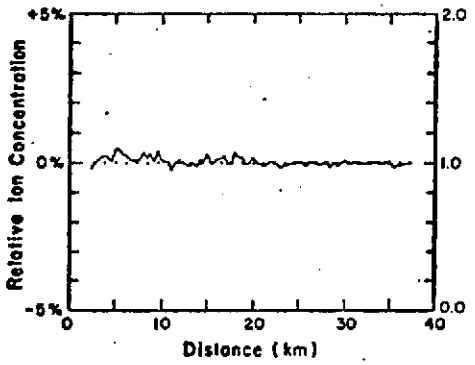

Fig. 8

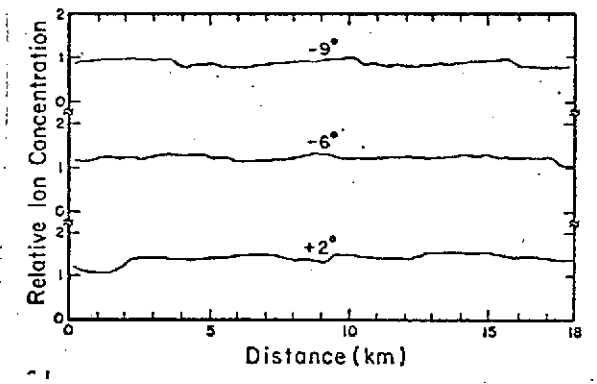

Fig. 9

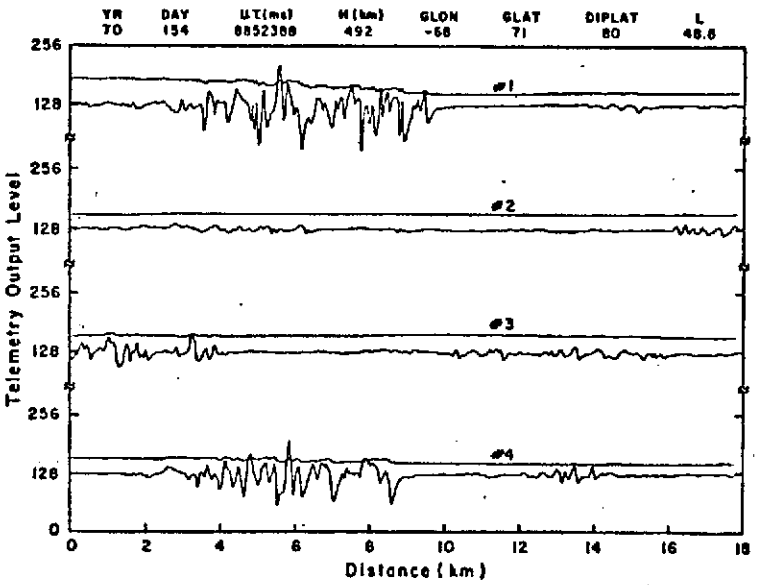

Fig. 10

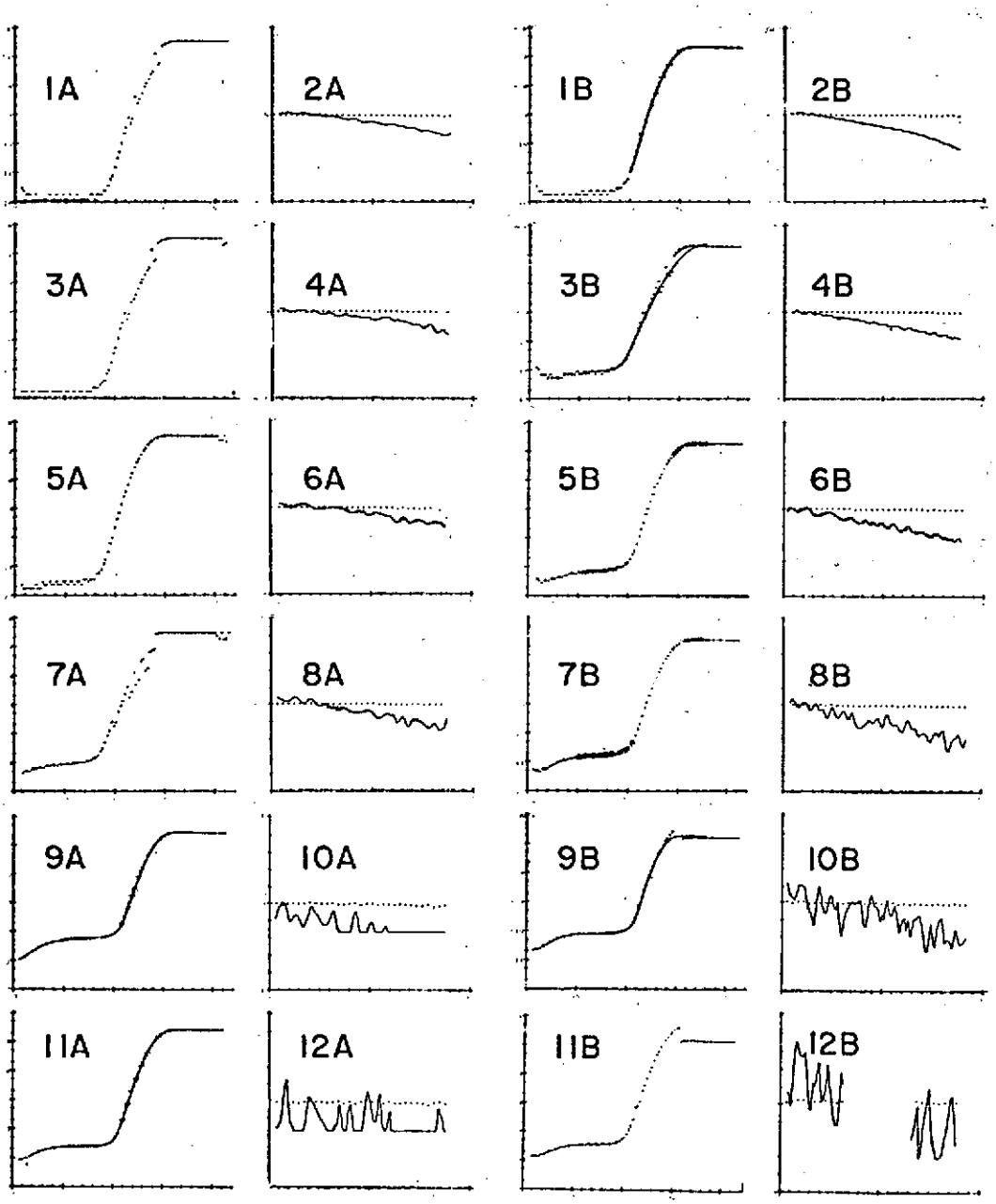

Fig. 7 (Final published size)

In-situ Measurements of Amplitude and Scale Size Characteristics of Ionospheric Irregularities

by

P. L. Dyson,* J. P. McClure and W. B. Hanson
The University of Texas at Dallas
Dallas, Texas 75230

*Permanent address: Physics Department
La Trobe University
Bundoora, Victoria, 3083
Australia

ABSTRACT

The retarding potential analyzer aboard Ogo 6 has provided high resolution observations of the ion concentration along the satellite path. Changes in ion concentration as small as .03% and at times .01% could be measured. Spatial resolution varied from 35 to 380 meters. Samples of data have been spectrally analyzed to determine the variation of irregularity amplitude with scale size. The most common spectrum observed is of the form $A \alpha S^n$ where A is the irregularity amplitude and S is the scale size. The spectrum was measured over the scale size range 70 m to 7 km and the values of n obtained were close to one, the average value being 0.95. The spectral index, n, is found to be insensitive to irregularity amplitude. This type of spectrum suggests that the irregularities in this scale size range result from the turbulent dissipation of larger irregularities. At the equator the larger irregularities are probably produced by convective electric fields. At high latitudes electric fields may also be involved but other factors such as precipitating particles may contribute to, or be primarily responsible for, the production of large irregularities. Examples of other types of spectra associated with wave-like irregularities and with "ground glass" (high frequency noise) irregularities are also shown.

Introduction:

Various properties of F-region irregularities have been studied by many workers over several decades. Even so, the processes responsible for producing irregularities are not yet completely understood. It is important to know the spatial extent (scale size) and plasma concentration changes (amplitude) of the irregularities in order to understand how they are generated; however, except in the case of travelling ionospheric disturbances (TID's), relatively little information of this type is available. Because TID's usually have quite large scale sizes (tens of kilometers or more) and produce a relatively simple "rippling" of the ionosphere, their dimensions can be determined by ground based radio techniques (e.g. Munro and Heisler, 1956; Thome 1964) as well as by in situ measurements (e.g. Harris et al., 1969; Dyson et al. 1970). However, the ionospheric structure is more complex when spread F or radio scintillation occur, and it is difficult to obtain unambiguous information about the characteristics of the irregularities from ground based radio techniques. Some results have been obtained from radio star observations (Elkins and Papagiannis, 1969; Rufenach 1971, 1972) and indicate that the spectrum of irregularity amplitude versus scale size obeys a power law over the scale size range 0.6 to 4 km. Unfortunately it appears that Fresnel filtering effects prevent information being obtained at other scale sizes. Similarly previous in situ measurements (Dyson 1969, 1971) have been restricted to a limited scale size and amplitude range ($\sim$ 1 km and $\geq$ 5%).

The Ogo-6 retarding potential analyzer (RPA) experiment has a mode of operation, called the duct mode, which is specifically designed to measure the amplitude and scale sizes of ionospheric irregularities (Hanson et al. 1970). Changes in ion concentration as small as .03%, and at times at small as .01%, can be measured. On occasions telemetry rates enabled the ion concentration to be measured every 35 meters along the satellite path. Examples of the various types of ionospheric structure detected by the Ogo 6 RPA have been presented by McClure and Hanson (1973). In this paper we present quantitative results of the amplitude-scale size characteristics of different types of structure and discuss the significance of the results.

Results:

The variation of irregularity amplitude with scale size has been determined by power spectrum analysis techniques. The data from the RPA is in the form of electrometer voltage (which is proportional to ion concentration) as a function of time. Each section of data to be spectrally analyzed was first detrended by removing the linear variation as given by the line of best fit (see Fig. 1). Spectral estimates were then calculated by the fast Fourier transform (FFT) technique (Cooley and Tukey, 1965). Spectral smoothing was usually achieved by averaging over a number of consecutive spectral estimates. This method was used for data obtained at special data rates which gave spatial resolutions of either 35 or 140 meters.

Generally duct mode data were obtained during alternate 5 second or 20 second intervals and with a spatial resolution of 380 m. For this data spectral smoothing was achieved by averaging spectral estimates from adjacent sections of duct mode data. The input to the FFT was a time series of values of ΔV (see Figure 1). The Fourier spectra are presented here with scales of spectral intensity vs frequency and also with scales of equivalent irregularity amplitude vs scale size. The satellite velocity was divided by the frequency to provide a length scale. The units of the spectral intensity and equivalent amplitude scales are Hz^{-1} and $Hz^{-1/2}$, respectively. The intensity scales are unnormalized (arbitrarily normalized), and the amplitude scales are normalized as follows: the FFT output in each frequency window was converted to the percentage RMS amplitude $\Delta N_{RMS}/\bar{N}(\%)$ equivalent to the total fluctuation power in the given window.

The most detailed measurements of ionospheric structure were obtained when, during a number of orbits, the total ion concentration was measured continuously every 35 m along the satellite path. Two of these, orbits 5147 and 6412 which occurred on May 27 and August 24, 1970, respectively, have been analyzed in detail. When the satellite was within typical irregularity regions on these and other orbits the

measured ion concentration variations were similar in form to those shown in Figure 1. Spectra were calculated at various latitudes using several different record lengths. An example is shown in Figure 2. This spectrum was derived from 9.6 seconds of data (2048 data points). The spectrum is well defined over two orders of magnitude of scale size from 70 meters upward and is very linear when plotted with logarithmic scales. The spectrum has a slope of $0.92 \pm .06$ (the slope of the power spectrum would be twice this value). In calculating the error in slope, the known variance of each spectral point has been taken into account using the method outlined by Bendat and Piersol (1966). This spectrum is typical of those observed on orbits 5147 and 6412, viz., that the spectrum obeys a power law of index very close to one; i.e., the amplitude of the irregularities is approximately proportional to the scale size. The most obvious difference between spectra obtained from different record segments is that the absolute value of the amplitude at a given scale size depends on the RMS amplitude of the data segment. For the two orbits under discussion, spectra have been calculated at different locations along the orbital path using record lengths of 4.8 sec ($\sim$35 km) and 9.6 sec ($\sim$70 km). The values obtained for the spectral slope or index are plotted in Fig. 3 as a function of invariant latitude. The points with the larger error bars are for the 4.8 sec segments of data. There are no significant changes in the spectral index as a function of latitude. The average value is different for the two passes but not significantly so. The data were collected at local times between 20

and 10 hrs., i.e. between 8 P.M. and 10 A.M. The local time of course changes rapidly at high latitudes where longitude changes rapidly along the satellite path.

During orbit 7729 on November 20, 1970, measurements of ionospheric structure in the equatorial region were made with a spatial resolution of 140 meters during alternate 4.8 second periods. Again the measured ion concentration variations are similar in form to that shown in Figure 1 and one of the calculated spectra is shown in Figure 4. The scale sizes have been converted to equivalent scale size perpendicular to the magnetic field direction so that although the spatial resolution along the orbital path is 140 meters, this is equivalent to $\sim$40 meters perpendicular to the magnetic field direction for the example in Figure 4. The spectrum has the same form as those obtained at middle and high latitudes, i.e., it is a power law of index close to one. However, because of the lower sampling rate and shorter record length available, the spectrum is only defined over one and a half decades and there is greater uncertainty in the slope. Again this spectrum is typical of those observed throughout the irregularity region and the values of spectral index obtained in the equatorial region are listed in Table 1.

The type of ion concentration variation along the satellite path which is shown in Figures 2 and 4 is the most common type of ionospheric structure observed (McClure and Hanson, 1973) implying that generally within ionospheric irregularity regions the irregularity amplitude increases almost linearly with the scale size. A further demonstration of the relative constancy of the power law index is given in Figure 5

where the spectral index data of Figure 3 is plotted as a function of the percentage RMS amplitude of the ion concentration variations. There is no significant change in the spectral index even though the RMS amplitude of $\Delta N/N$ at a given scale size varies over more than two orders of magnitude. An average value of spectral index of 0.95 is obtained by combining the data of Figure 3 and Table 1.

Other types of irregularity structure are observed but not as frequently as the type discussed above. Occasionally near the equator wave-like variations in ion concentration are observed. Two examples are shown in Figure 6 together with the calculated spectra. (In this figure the scale sizes are those along the orbital path.) The two spectra differ in that in one case power is contained within a limited scale size band whereas in the other example the waveform is comprised of a fundamental plus harmonics. The scale size of the fundamental is 7.5 km and it is presumably at this scale size that the energy input occurs for the production of the irregularities.

A third category of irregularities, called "ground glass" by McClure and Hanson (1973) is illustrated in Figure 7. It is apparent from the ion concentration measurements that the irregularities are primarily small scale although, in this example, some relatively large scale sizes are present as evidenced by the amplitude modulation of the ground glass which is particularly noticeable in the first two segments of data. The larger scale sizes are not typical of the ground glass phenomena and have been filtered from the data so that the spectrum

in Figure 7 is for the higher frequency variations evident in the data. The spectrum shows a random variation of power with scale size; i.e. the "ground glass" appears to be white noise with scale sizes smaller than about 3 km.

Discussion:

The most striking features of the power law spectra are the relatively constant spectral index over more than two orders of magnitude of scale size and also over more than two orders of magnitude of percentage RMS amplitude of the ion concentration variations. These properties are consistent with the hypothesis that the irregularities are produced by turbulence over the measured region of scale sizes (70 m to 7 km). The suggested mechanism is that initially irregularities are generated at some large scale size or sizes and the dissipation of the energy associated with these irregularities occurs by generating smaller and smaller irregularities. The fact that the power law spectra continues down to scale sizes of 70 meters or less indicates that the final dissipation of energy occurs at scale sizes smaller than this.

At the large scale size end of the spectrum the amplitude cannot keep increasing indefinitely with scale size and in fact the irregularity amplitude must approach zero at scale sizes larger than that at which energy is fed into the turbulence. Thus it might be expected that by taking longer record lengths and extending the spectra to larger scale sizes the scale sizes at which energy is fed into the irregularities could be determined. However, this is probably not worth pursuing for the following reasons. Firstly, only a one-dimensional spectrum can be

obtained and such spectra are subject to aliasing at large scale sizes. This arises because in a turbulent medium the larger scale sizes are not isotropically distributed so that if the contours of these irregularities are not perpendicular to the satellite velocity they will appear to have a larger than actual scale size (Tennekes and Lumley, 1972). Secondly, there are geophysical reasons for limiting the length of records used. At high latitudes quite rapid changes in the background ion concentration can occur in trough and auroral regions. If record lengths longer than $\sim$100 km are used then it is likely that the spectra will contain the effects of ion concentration changes produced by processes not related to the irregularities. Since irregularities in the F region are field-aligned, record lengths near the equator should be sufficiently short so that the dip angle does not change appreciably.

In the equatorial region electric fields are probably the source of the turbulence. Cole (1971) has shown that in the equatorial region plasma convection generated by E-region electric fields will produce F-region irregularities with scale sizes of $\sim$10 km or greater perpendicular to the magnetic field direction. Following the surprising discovery of Hanson and Sanatani (1971) that equatorial irregularities are related to the presence of Fe^+, Hanson et al. (1973) suggested that the convective electric fields are produced as follows. The irregular concentration of metallic ions below the F layer produces variations in the integrated Pedersen conductivity along the equatorial field lines. Then the effect of neutral winds in the region of conductivity structure is to produce

the electric fields which produce large scale irregularities ($\gtrsim$ 10 km). Thus relatively large scale gradients in electric field and ion concentration will be present and either or both could generate the turbulence which produces the smaller scale size irregularities. Electrostatic turbulence at the equator has been measured in a region of spread F (McClure and Woodman, 1972) and satellite measurements indicate that the spectrum of the electrostatic turbulence (Kelley and Mozer, 1972b) obeys a similar power law to that reported here for the ion concentration variations.

At high latitudes electric fields may also be responsible for the production of irregularities particularly in and near the auroral oval. However there are other possible sources in the oval region. For example, the combined heating and ionization effects of precipitating particles may produce the large scale irregularities which initiate the turbulence. Electrostatic turbulence does occur in this region and has a similar power law to that of the ion concentration irregularities (Kelley and Mozer, 1972a).

The deduction of a power law spectrum is very pertinent to ionospheric scintillation observations, particularly those at Gigahertz frequencies (Pope and Fritz, 1970; Skinner et al., 1971). Scintillation at these frequencies was expected to be much smaller than is observed. However, calculations were based on a Gaussian spectrum rather than a power law one. Compared to a Gaussian spectrum, a power law spectrum contains significantly higher spectral densities at the smaller scale sizes and hence implies a slower fall off in scintillation index with increasing frequency as is observed. The explanation given by McClure

and Hanson (1973) of the fact that the scintillation index at Gigahertz frequencies is greater at the equator than in the auroral regions is reinforced by the spectral results obtained here. At the equator at night N_e is larger than in the auroral regions but Ogo 6 results show that both the percentage amplitude of the irregularities and the spectrum of the irregularities are similar in the two regions. Hence the absolute amplitude, which is the significant parameter for scintillation, is larger at the equator and so larger scintillation effects would be expected in this region.

The spectra shown in Figures 6 and 7 demonstrate interesting departures from the more frequently observed power law spectrum. It is conceivable that these spectra indicate different phases of the processes responsible for the power law spectra. For example, the wave-like structures may represent the situation before dissipation by turbulence begins and the spectrum of Fig. 7 could be indicative of the decay of the irregularities after the feeding in of energy at the large scale sizes has stopped. Of course this is very speculative and the fact that the wave-like structure occurs near the equator and "ground-glass" irregularities are a mid-latitude phenomena argues against this. The wave-like irregularities may be manifestations of gravity waves; if so they are smaller in amplitude and wavelength than are usually observed by radio techniques. Further investigations are needed to determine the real significance of the wave-like and ground glass irregularities.

Conclusions:

For F-region irregularities, generally the irregularity amplitude is very nearly proportional to the irregularity scale size over the range 70 meters to 7 km; i.e., the gradients in ion concentration are independent of wavelength. The interpretation of this spectral form is that irregularities are initially generated at large scale sizes ($\sim$10 km), become unstable and dissipate their energy by generating smaller sized irregularities as in turbulence. In the equatorial region the large scale irregularities are most likely produced by convective electric fields. At high latitudes electric fields may also be responsible; however other phenomena such as precipitating particles may be primary or contributary causes.

This power law spectrum, when considered with the appropriate ionospheric parameters, probably explains the observations of radio scintillation at gigahertz frequencies both at the equator and in the auroral regions. The power law index is shown to be independent of the total RMS amplitude over a range of two orders of magnitude. Three other types of spectra have also been presented, two of which are associated wave-like variations in ion concentration. One of these spectra has the energy confined to a narrow band of scale sizes and the other consists of a fundamental scale size plus harmonics. The remaining spectrum has power randomly distributed over scale sizes smaller than about 3 km.

Acknowledgments:

This work was supported by NSF Grant GA-31318 and by NASA under Grant NGL-44-004-001 and contracts NAS 5-9311 and NAS 5-23184. One of us (P.L.D.) is indebted to LaTrobe University for leave to carry out this work.

Table 1: Values of spectral index obtained during orbit 7729 on 20 November 1970

Dip Latitude (Degrees)	Spectral Index (± 0.28)
-11.0	1.00
-10.5	1.26
-10.0	1.04
- 9.5	1.13
- 7.0	1.08
5.0	1.15
6.0	1.12

References

Bendat, J. S., and A. G. Piersol, Measurement and analysis of random data, John Wiley and Son, New York, 1966, p. 227

Cole, K. D., Formation of field-aligned irregularities in the magnetosphere, J. Atmos. Terr. Phys., 33, 741, 1971

Cooley, J. W., and J. W. Tukey, An algorithm for the machine calculation of complex Fourier series, Math. of Computations, 19, 297, 1965

Dyson, P. L., Direct measurements of the size and amplitude of irregularities in the topside ionosphere, J. Geophys. Res., 74, 6291, 1969

Dyson, P. L., On the significance of electrostatic probe observations of electron density irregularities, J. Geophys. Res., 76, 4689, 1971

Dyson, P. L., G. P. Newton, and L. H. Brace, In situ measurements of neutral and electron density wave structure from the Explorer 32 satellite, J. Geophys. Res., 75, 3200, 1970

Elkins, T. J., and M. D. Papagiannis, Measurement and interpretation of power spectrums of ionospheric scintillation at a sub-auroral location, J. Geophys. Res., 74, 4105, 1969

Hanson, W. B., S. Sanatani, D. Zuccaro, and T. W. Flowerday, Plasma measurements with the retarding potential analyzer on Ogo 6, J. Geophys. Res., 75, 5483, 1970

Hanson, W. B., J. P. McClure, and D. L. Sterling, On the cause of equatorial spread F, J. Geophys. Res., 78, 2353, 1973

Harris, K. K., G. W. Sharp, and W. C. Knudsen, Gravity waves observed by ionospheric temperature measurements in the F region, J. Geophys. Res., 74, 197, 1969

Kelley, M. C., and F. S. Mozer, A satellite survey of vector electric fields in the ionosphere at frequencies of 10 to 500 hertz, 1, isotropic, high-latitude electrostatic emissions, J. Geophys. Res., 77, 1972a

Kelley, M. C., and F. S. Mozer, A satellite survey of vector electric fields in the ionosphere at frequencies of 10 to 500 hertz, 3, low-frequency equatorial emissions and their relationship to ionospheric turbulence, J. Geophys. Res., 77, 4183, 1972b

McClure, J. P., and W. B. Hanson, A catalog of F-region ionospheric irregularity behavior based on Ogo-6 retarding potential analyzer data, accepted for publication, J. Geophys. Res., 1973

McClure, J. P., and R. F. Woodman, Radar observations of equatorial spread F in a region of electrostatic turbulence, J. Geophys. Res., 77, 5617, 1972

Munro, G. H., and L. H. Heisler, Cusp-type anomalies in variable frequency ionospheric records, Aust. J. Phys., 9, 343, 1956

Pope, J. H., and R. B. Fritz, Observations of simultaneous scintillation on VHF and S-band satellite transmissions at high latitudes, NOAA Tech. Rep. ERL 207-OD 6, U. S. Govt. Print. Office, Washington, D.C., 1970

Rufenach, C. L., A radio scintillation method of estimating the small-scale structure in the ionosphere, J. Atmos. Terr. Phys., 33, 1941, 1971

Rufenach, C. L., Power-law wavenumber spectrum deduced from ionospheric scintillation observations, J. Geophys. Res., 77, 4761, 1972

Skinner, N. J., R. F. Kelleher, J. B. Hacking, and C. W. Benson, Scintillation fading of signals in the SHF band, Nature Phys. Sci., 232, 19, 1971

Tennekes, H., and J. L. Lumley, A first course in turbulence, MIT Press, Massachusetts, 1972, p. 248

Thome, G. D. Incoherent scatter observations of travelling ionospheric disturbances, J. Geophys. Res., 69, 4047, 1964

Figure Captions

Fig. 1. Detrending of data before spectral analysis

Fig. 2. Irregularity spectrum for 9.6 sec of data obtained during orbit 5147 on 27 May 1970.

Fig. 3. Spectral index as a function of invariant latitude for orbits 5147 and 6412 which occurred on 27 May and 24 August 1970, respectively

Fig. 4. Irregularity spectrum for 4.8 sec of data obtained during orbit 7729 on 20 November 1970

Fig. 5. Spectral index as a function of percentage RMS ion concentration for orbits 5147 and 6412

Fig. 6. Irregularity spectra for
(a) orbit 7905 on 2 December 1970
(b) orbit 2391 on 18 November 1969

Fig. 7. Irregularity spectrum for orbit 2395 on 18 November 1969

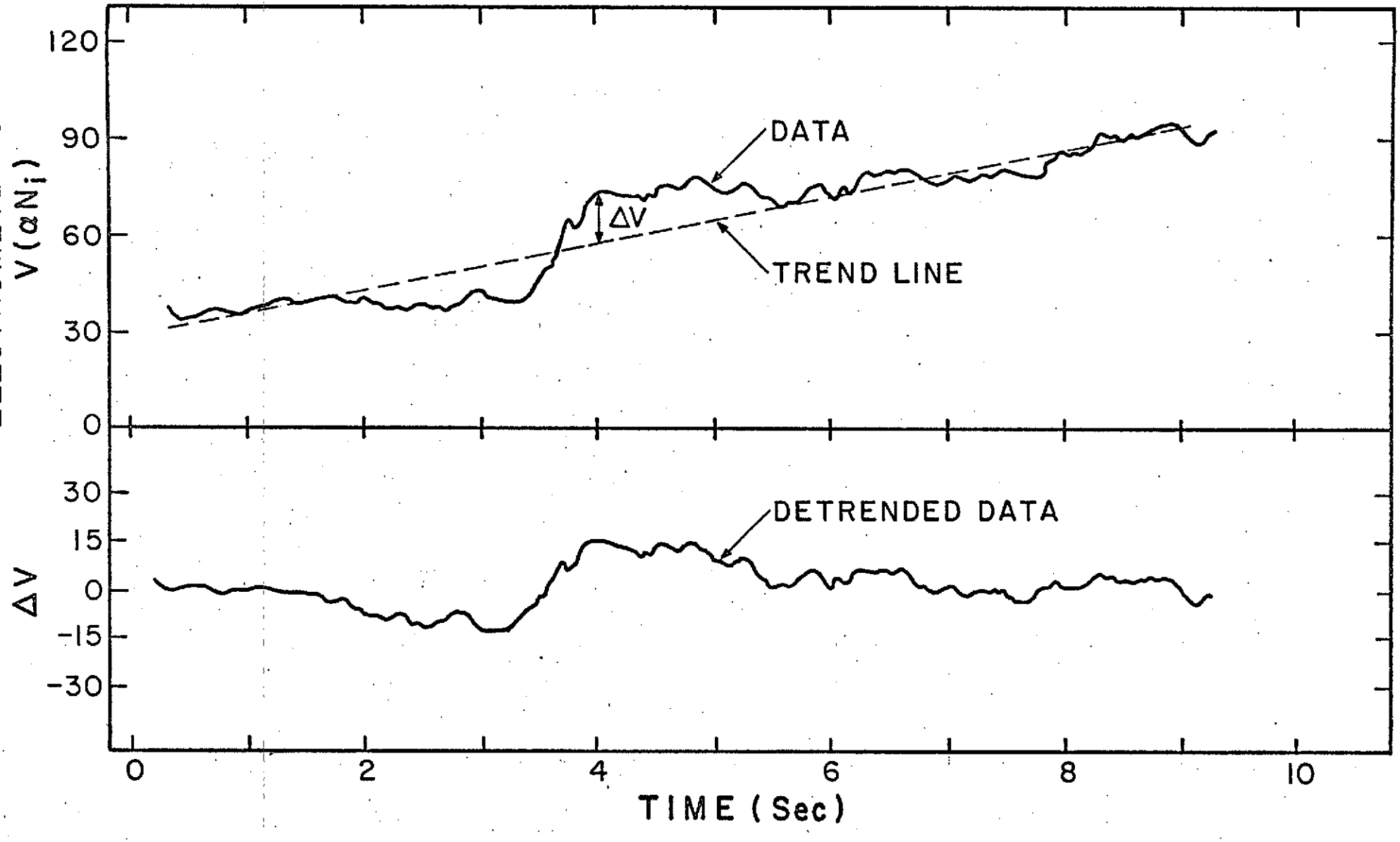
ELECTROMETER OUTPUT
V (αN_i)
120
90
60
30
0
DATA
ΔV
TREND LINE
30
15
0
-15
-30
ΔV
DETRENDED DATA
0
2
4
6
8
10
TIME (Sec)

FIGURE 1

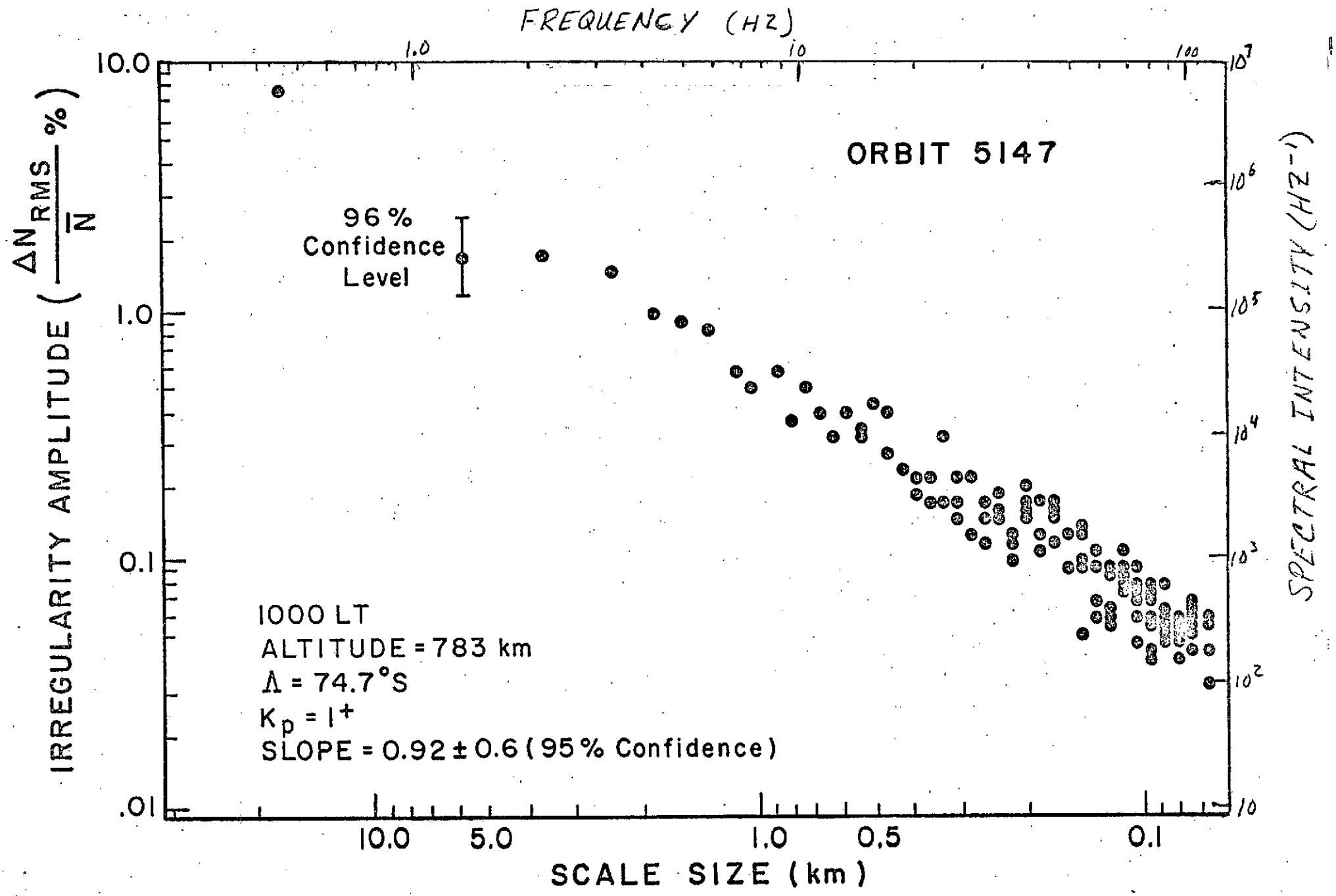
FREQUENCY (HZ)
1.0
10
100
ORBIT 5147
96 %
Confidence
Level
1000 LT
ALTITUDE = 783 km
Λ = 74.7°S
$K_p = 1^+$
SLOPE = 0.92 ± 0.6 (95 % Confidence)
IRREGULARITY AMPLITUDE $\left(\frac{\Delta N_{RMS}}{\bar{N}}\ \%\right)$
10.0
1.0
0.1
.01
SPECTRAL INTENSITY (HZ^{-1})
10^7
10^6
10^5
10^4
10^3
10^2
10
10.0
5.0
1.0
0.5
0.1
SCALE SIZE (km)

FIGURE 2

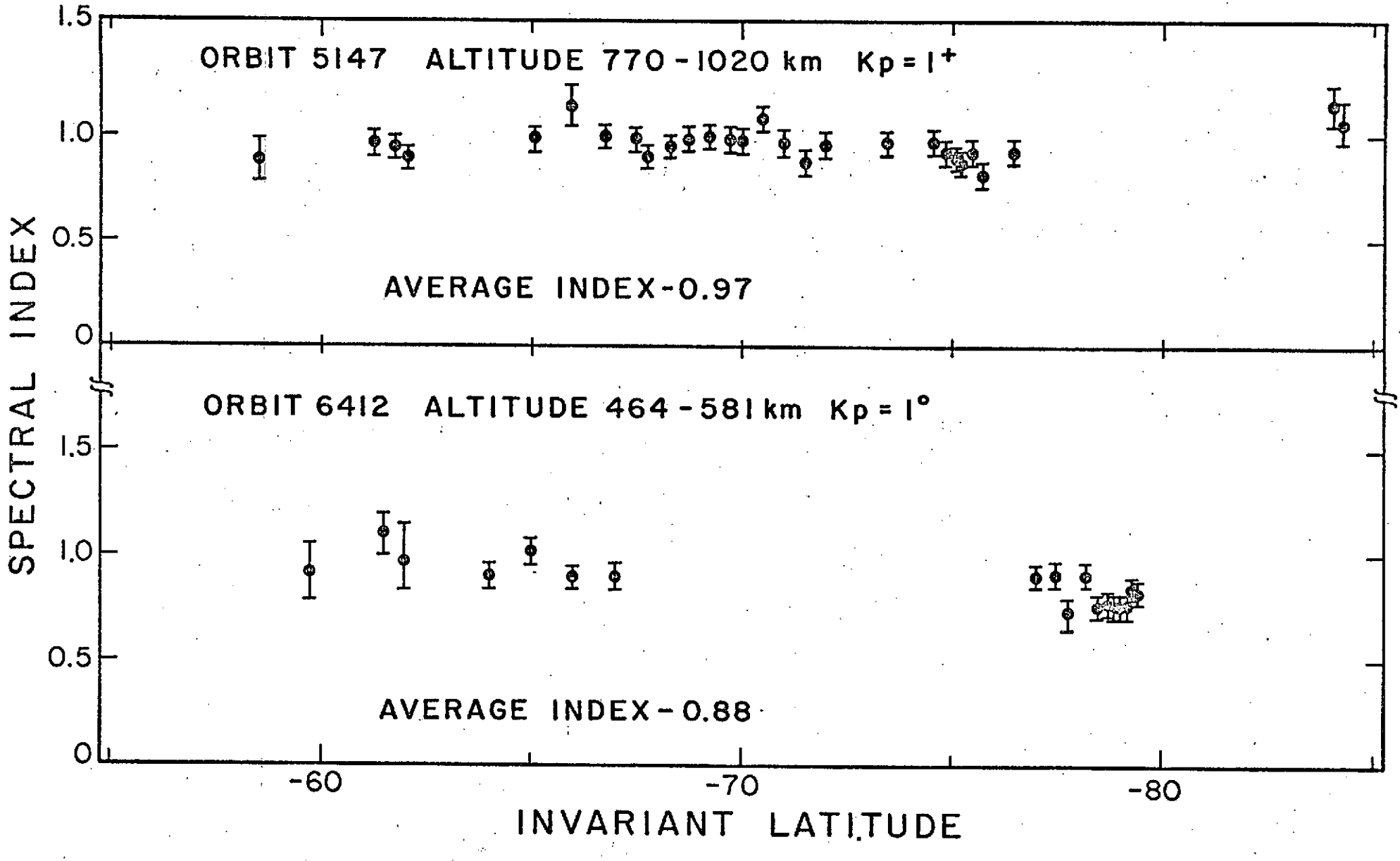
ORBIT 5147 ALTITUDE 770 - 1020 km Kp = 1+
AVERAGE INDEX - 0.97
ORBIT 6412 ALTITUDE 464 - 581 km Kp = 1°
AVERAGE INDEX - 0.88
SPECTRAL INDEX
1.5
1.0
0.5
0
-60
-70
-80
INVARIANT LATITUDE

FIGURE 3

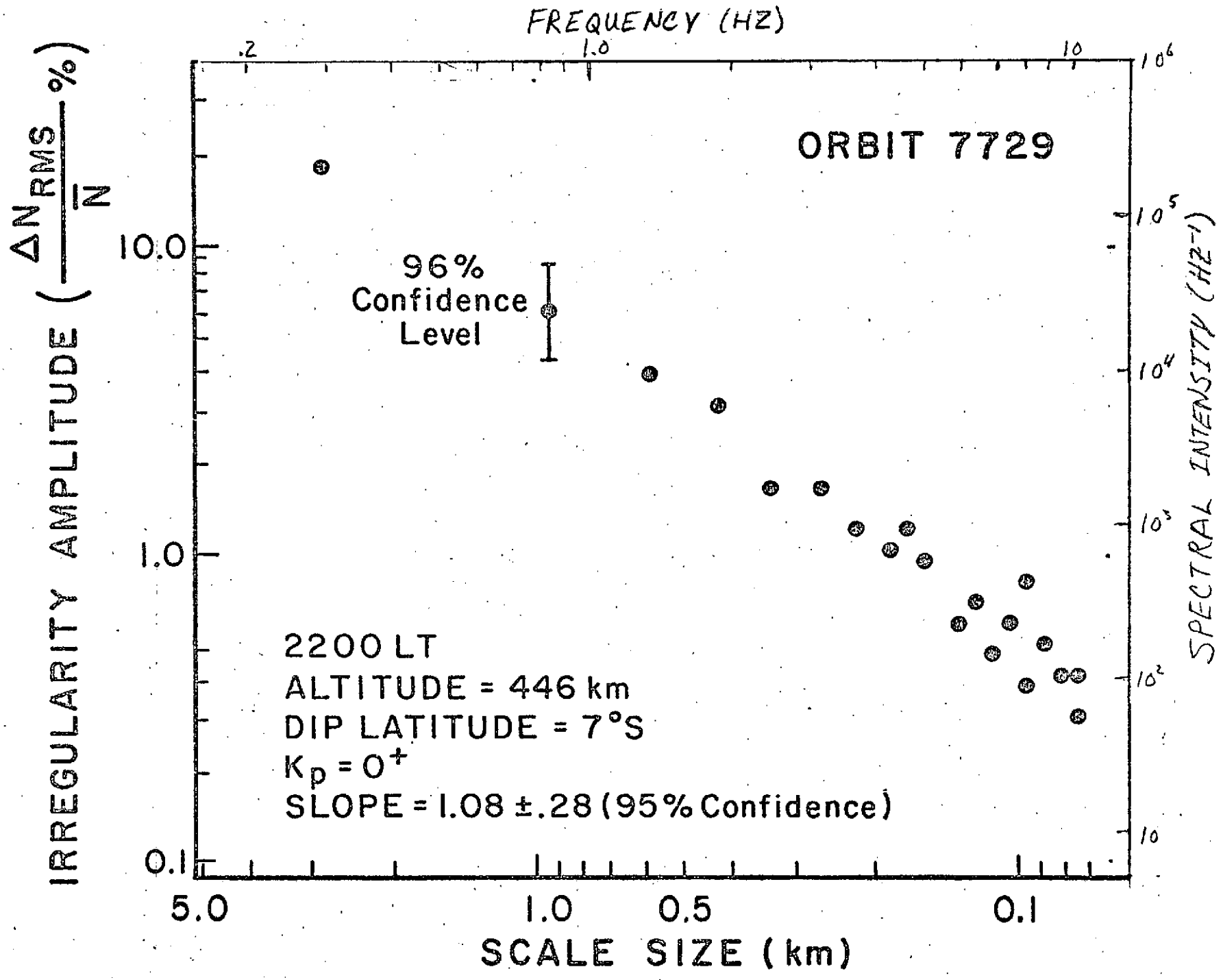
FREQUENCY (HZ)
.2
1.0
10
ORBIT 7729
96%
Confidence
Level
2200 LT
ALTITUDE = 446 km
DIP LATITUDE = 7°S
$K_p = 0^+$
SLOPE = 1.08 ±.28 (95% Confidence)
IRREGULARITY AMPLITUDE $\left(\frac{\Delta N_{RMS}}{\bar{N}} \%\right)$
10.0
1.0
0.1
5.0
1.0
0.5
0.1
SCALE SIZE (km)
SPECTRAL INTENSITY (HZ-1)
10^6
10^5
10^4
10^3
10^2
10

FIGURE 4

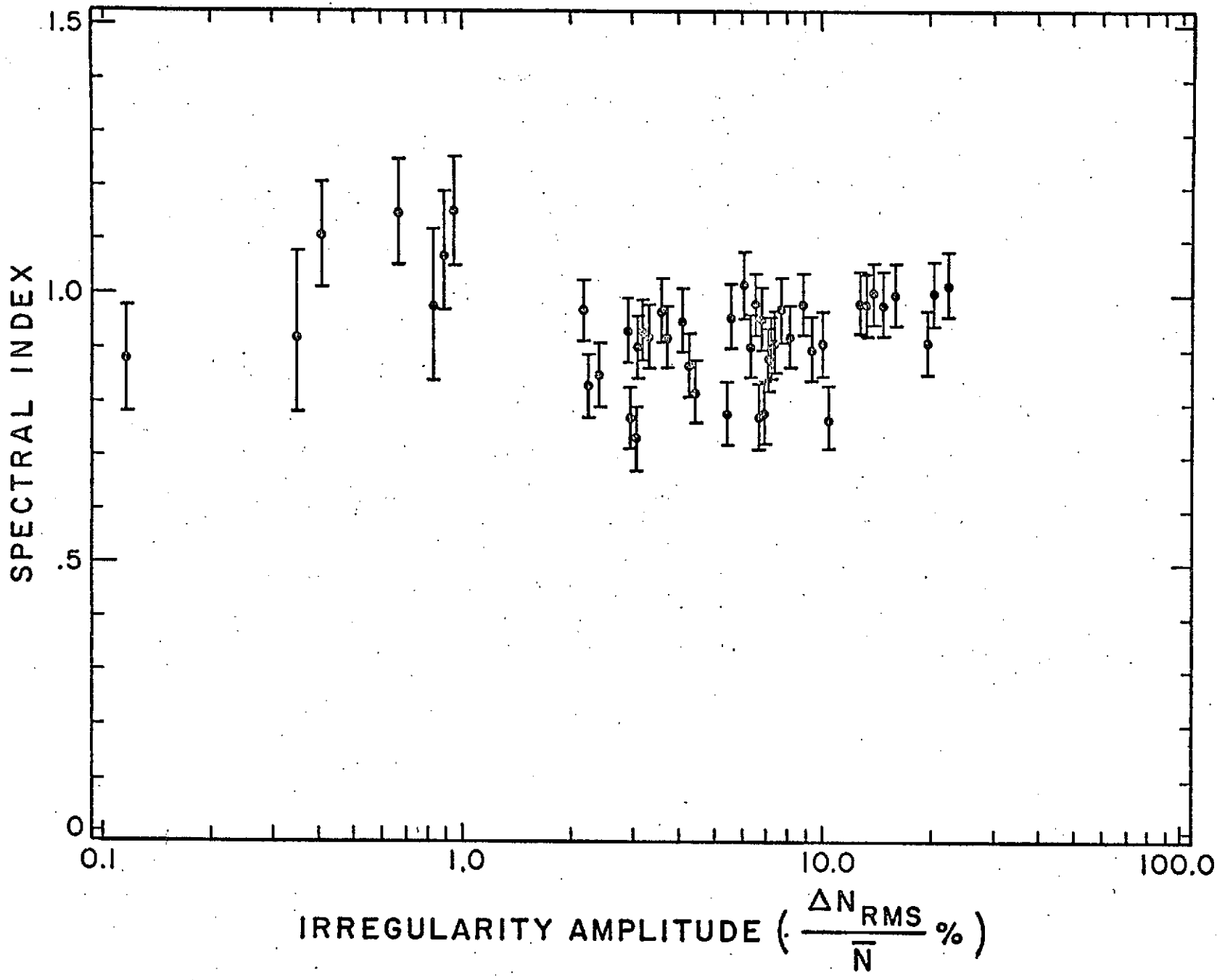
1.5
1.0
.5
0
SPECTRAL INDEX
0.1
1.0
10.0
100.0
IRREGULARITY AMPLITUDE ($\frac{\Delta N_{RMS}}{\bar{N}}$ %)

FIGURE 5

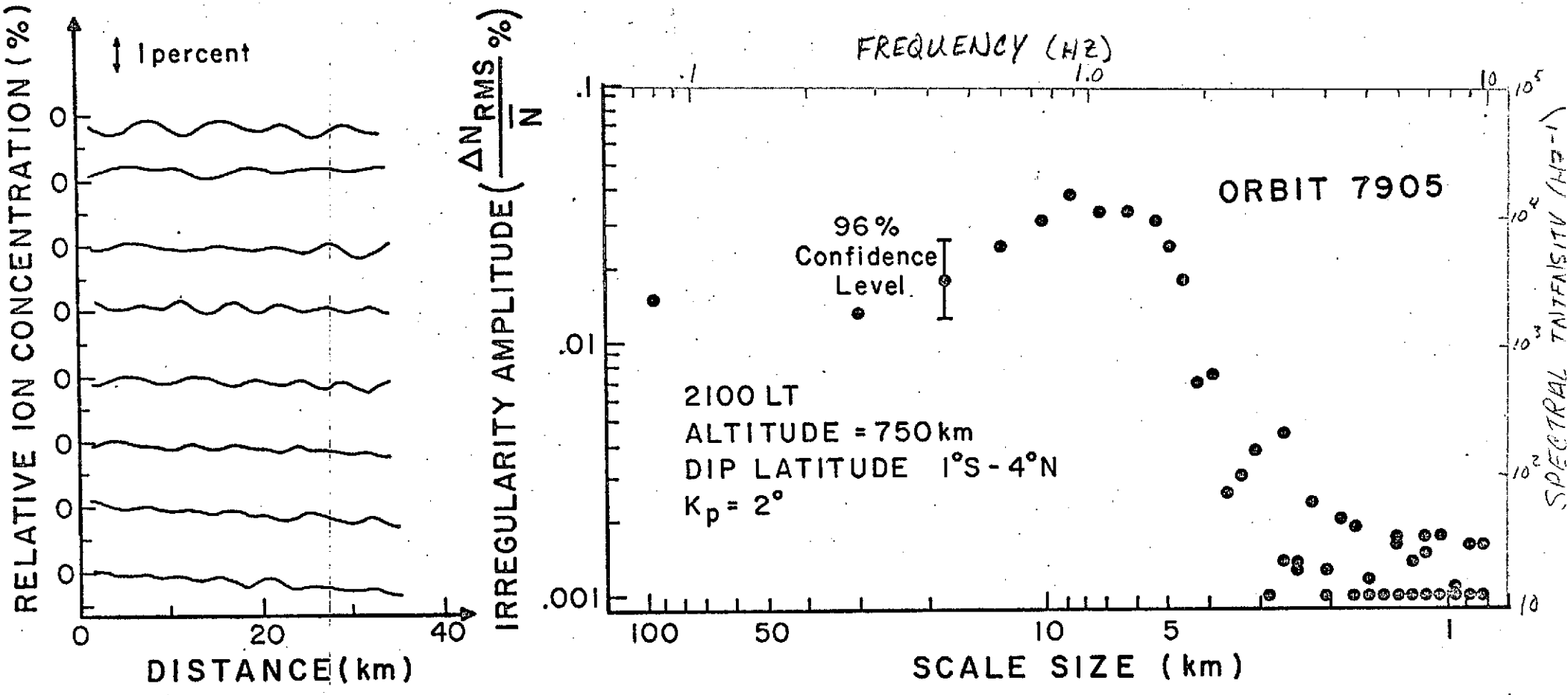
RELATIVE ION CONCENTRATION (%)
1 percent
0
20
40
DISTANCE (km)
IRREGULARITY AMPLITUDE ($\frac{\Delta N_{RMS}}{\overline{N}}$ %)
FREQUENCY (HZ)
.1
1.0
10
.1
.01
.001
ORBIT 7905
96% Confidence Level
2100 LT
ALTITUDE = 750 km
DIP LATITUDE 1°S - 4°N
K_p = 2°
100
50
10
5
1
SCALE SIZE (km)
SPECTRAL INTENSITY (M²-1)
10^5
10^4
10^3
10^2
10

FIGURE 6a

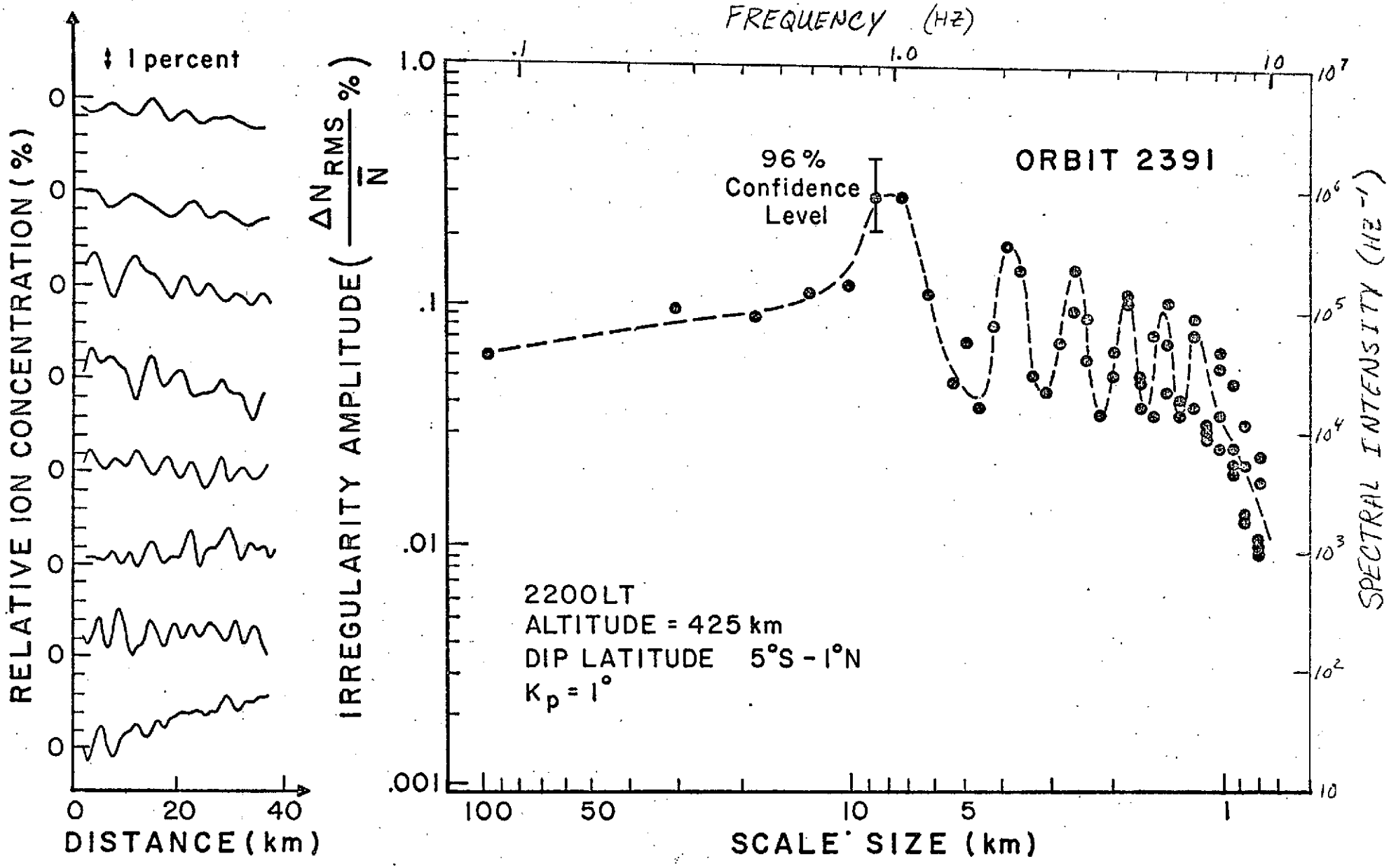
FREQUENCY (HZ)
.1
1.0
10
1 percent
RELATIVE ION CONCENTRATION (%)
0
0
0
0
0
0
0
0 20 40
DISTANCE (km)
IRREGULARITY AMPLITUDE ($\frac{\Delta N_{RMS}}{\bar{N}}$ %)
1.0
.1
.01
.001
96% Confidence Level
ORBIT 2391
2200 LT
ALTITUDE = 425 km
DIP LATITUDE 5°S - 1°N
K_p = 1°
100 50 10 5 1
SCALE SIZE (km)
SPECTRAL INTENSITY (HZ^{-1})
10^7
10^6
10^5
10^4
10^3
10^2
10

FIGURE 6b

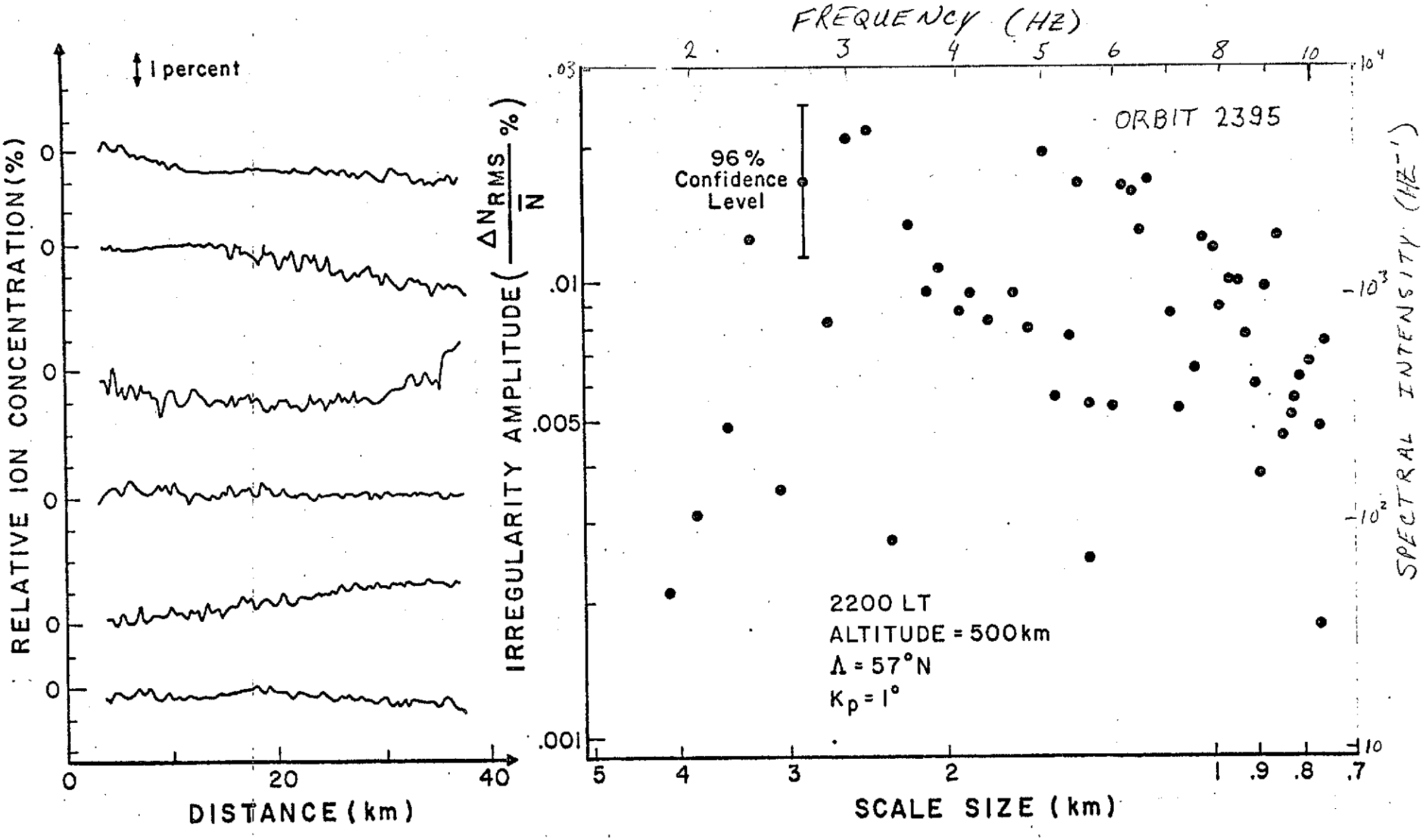
1 percent
RELATIVE ION CONCENTRATION (%)
0
0
0
0
0
0
0
20
40
DISTANCE (km)
FREQUENCY (HZ)
2
3
4
5
6
8
10
10^4
.03
.01
.005
.001
IRREGULARITY AMPLITUDE $\left(\frac{\Delta N_{RMS}}{\bar{N}}\ \%\right)$
96 % Confidence Level
ORBIT 2395
2200 LT
ALTITUDE = 500km
Λ = 57°N
K_p = 1°
5
4
3
2
1
.9
.8
.7
SCALE SIZE (km)
10^3
10^2
10
SPECTRAL INTENSITY (HZ^{-1})

FIGURE 7

TOPSIDE IONOSPHERIC SPREAD F AND PARTICLE PRECIPITATION IN THE DAYSIDE MAGNETOSPHERIC CLEFTS

by

P. L. Dyson,
La Trobe University,
Bundoora, Victoria,
Australia, 3083

and

J. D. Winningham,
University of Texas at Dallas,
Dallas, Texas 75230

ABSTRACT

At high latitudes topside ionospheric spread F is observed over a very large latitude range. Within this spread F region there is a severe topside irregularity zone (stiz) in which irregularities have larger amplitudes than elsewhere. Topside ionograms obtained within the stiz exhibit very severe frequency spread ($\gtrsim$ 1 MHZ) at zero range. The stiz occurs up to altitudes of at least 3000 km. Its equatorward edge is quite abrupt and is a good reflector of HF radio waves. Echoes from the stiz boundary have been observed by satellites as far as 2500 km equatorward. Comparisons of simultaneous topside sounder and particle data indicate that on the dayside of the earth the equatorward boundaries of the stiz and of $\lesssim$ 300 eV electron precipitation coincide. It is clear that the ionizing and heating effects of the particle precipitation produce irregularities, but other processes may also contribute. Usually the stiz extends beyond the poleward boundary of the particle precipitation. This is probably due to magnetospheric convection transporting irregularities poleward of the region of production.

INTRODUCTION

Two distinct types of topside ionospheric spread F are generally acknowledged, viz. aspect-sensitive scattering and ducting. Their occurrence characteristics have been studied by Calvert and Schmid (1964), Hice and Frank (1966) and Dyson (1968). Various sub-classes may be recognized within these two major classifications. In particular, at high latitudes, scattering spread F may become so severe that the ionogram trace at the satellite height (i.e. at zero range) is spread in frequency the order of one megahertz (Petrie, 1966). An example of this phenomenon is shown in Figure 1a. For comparison a high latitude ionogram without severe spreading at the satellite height is shown in Figure 1b. This type of severe spread F occurs in regions where the amplitude of the ionospheric irregularities of about 1 km in size is greater than 5% (Dyson, 1969; 1971) and its occurrence characteristics are similar to those of auroral phenomena (Petrie, 1966). Evidence for the association of the severe spread F at the satellite height with particle phenomena has been given by Winningham et al. (1973b) who discussed in detail the observations obtained from the ISIS-2 experiments during a polar transit by that satellite. The severe spread F occurred in two zones, one on the dayside and one on the nightside, and the equatorward edges of these zones coincided with the equatorward edges of the cleft and the low-altitude plasma sheet respectively.

The ISIS-1 and 2 satellites offer an excellent opportunity to study the association between particle precipitation and spread F as they contain both topside sounder (Florida, 1969) and soft particle spectrometer (SPS) experiments (Heikkila et al., 1970). The SPS experiment is particularly suited to such a study because it covers a wide energy range for both electrons and

protons including those electron energies at which the interaction with the F region is most significant. In this paper we present results from these experiments which show that on the dayside of the auroral oval the severe spread F is intimately related to particle precipitation. For simplicity, the region in which severe topside ionospheric spread F at the satellite height is observed will be referred to as stiz (severe topside irregularity zone).

STIZ CHARACTERISTICS

In general, topside spread F has the following behaviour at middle and high latitudes. Ducting occurs at the low latitude edge of the spread F region. Scattering begins at a somewhat higher latitude and quickly becomes the predominant form. Such behaviour is observed regularly even during the daytime (Dyson, 1968). The stiz occurs within the region of scattering spread F, i.e. the stiz is not an isolated region of ionospheric irregularities but is contained within a region of irregularities which has a much greater latitudinal extent than the stiz itself. However the stiz can be readily discerned from this larger region of scattering spread F. The evidence for this is two-fold.

Firstly, the onset of the severe spreading at the satellite height, which characterizes the stiz, is usually quite distinct, i.e. it is obviously present on one ionogram but not an adjacent one. An example is shown in Figure 1 which shows two consecutive ionograms taken 30 secs apart (1.2°Λ lat.). Secondly, the equatorward edge of the stiz is usually sufficiently sharp and well defined to act as a reflecting surface for HF radio waves. Consequently the sounder detects echoes from the stiz boundary long before the satellite reaches the stiz region. Two types of echo are observed in this manner and they may be classified as short range and long range echoes

depending on whether the virtual range is less than or greater than that of the vertical incidence echoes. Examples are shown in Figure 2. The leading edge of the short range echo (Figure 2a) is clearly defined and exhibits some retarding at low frequencies but very little retarding at the higher frequencies. This fact together with the severe diffuseness of the traces beyond the leading edge suggests that the echoes are due to partial reflections from the stiz. If total reflection were responsible the short range echo trace would show evidence of retardation at the high frequency end corresponding to reflection from near the irregularity maximum electron density. Significant partial reflection occurs when the refractive index changes appreciably within one wavelength and hence the stiz must have a boundary of $\sim$ 150 m or less thick since echoes are usually observed at least up to 2 MHz.

The short (s) and long (ℓ) range echoes can be explained in the following way (Figure 3). If it is assumed that the stiz extends over a large height range in the F region, then the boundary of the stiz will be field-aligned and since the stiz occurs at high latitudes the stiz boundary will be nearly vertical. When the satellite is outside the stiz region then several return echoes will be observed by the sounder if the stiz boundary is sharp enough to cause reflection of radio waves. In addition to the usual vertical incidence echo (v echo), a direct "backscatter" echo from the stiz boundary will be observed (s echo) plus an echo due to oblique reflection in the ionosphere and at the stiz boundary (ℓ echo). When the satellite is closer to the stiz, these additional echoes will occur at a closer range. Once the satellite enters the stiz region the irregularities surrounding the satellite produce the severe spread F. The virtual ranges

of s and ℓ echoes observed on five ISIS-2 passes have been plotted in Figure 4. The horizontal scale is the time of the observations before (after) the satellite enetered (departed) the stiz and is effectively the distance from the stiz boundary. The stiz boundary is taken to be at the location of the most equatorward ionogram showing severe spread F at the satellite. As ionograms are obtained at 30 second intervals there is a zero error of up to this amount in the location of the stiz boundary. The five passes plotted in Figure 4 all show that the range of the stiz boundary echoes increases with increasing satellite distance from the stiz. The rate at which the range changes is different for the s and ℓ echoes and there is good agreement between the different passes. Taking the zero error into account, there is also quite good agreement between the actual ranges observed on each pass.

Several other features of Figure 4 are consistent with the propagation paths suggested in Figure 3. It is apparent from the geometry of Figure 3 that the range of the s echo should exhibit larger changes for a given change in satellite position than that of the ℓ echo. This is indeed the case and the change in range of the s echo is approximately equal to the change in satellite position (the dotted line has a slope equal to the satellite velocity). This is to be expected if the stiz boundary is nearly vertical (i.e. field aligned at high latitudes). At very large distances the ℓ echo range change should asymptotically approach the satellite position change and this is also observed in Figure 4. It is also apparent from Figure 3 that when the satellite is close to the stiz boundary, the s echo will be readily identifiable but the ℓ echo may be confused with the vertical incidence echo especially if the more usual forms of spread F are also present. Similarly when the satellite is more distant the ℓ echo will be easily identified but the s echo will be superimposed on the vertical incidence echoes. The observations shown in Figure 4 are consistent

with this explanation. It is worth noting that the "reflectivity" of the stiz boundary is such that echoes from it are often observed when the satellite is 2500 km away. Stiz has been observed by ISIS-1 at altitudes as high as 3000 km.

While the topside sounder readily locates the stiz it does not give definitive information on the characteristics of the irregularities themselves. It is known that the amplitude of irregularities in the 1 km size range is larger in the stiz region than at mid latitudes (Dyson, 1969, 1971). This has been confirmed with ISIS-2 data by comparing the sounder observations with simultaneous Langmuir probe observations. In the process an interesting new feature has been detected and is illustrated in Figure 5. When the percentage amplitude of the irregularities, as observed by the Langmuir probe, is compared with the sounder observations of the stiz, there is some disagreement particularly at about 0604 UT where large percentage irregularities (Figure 5c) were observed but no severe spread F (Figure 5a). If however the absolute amplitude (Figure 5b) of the irregularities is compared with the spread F observations, it is apparent that the stiz is coincident with the irregularities of largest absolute amplitude.

In order to understand this we need to consider the refractive index of the medium because the radio waves are affected by changes in refractive index rather than changes in electron concentration per se. Since the spread F in the stiz region is due to partial reflections, we can consider a frequency of propagation, f, much greater than the local plasma frequency. Thus we may write the refractive index, μ, as

$$\mu^2 = 1 - \frac{aN}{f^2}$$

where a is a constant and N is the electron concentration. From this expression we obtain the relation

$$\Delta\mu = \frac{-a\Delta N}{2f^2(1 - aN/f^2)^{\frac{1}{2}}}$$

For small values of N this becomes

$$\Delta\mu = \frac{-a\Delta N}{2f^2}$$

Thus changes in refractive index are proportional to the absolute change in electron concentration when the frequency of propagation is significantly greater than the plasma frequency. Hence the severe spread F associated with the stiz is indicative of the presence of irregularities of a certain absolute (rather than percentage) amplitude.

Comparison of Stiz and Particle Precipitation

It has often been suggested that particle precipitation is responsible for the production of ionospheric irregularities in the auroral regions. Previous studies have shown that the occurrence of stiz is similar to that of various auroral phenomena (Petrie, 1966; Dyson, 1969).

The present electron precipitation-ionospheric irregularity study is a continuation of earlier work by Winningham (1970), Heikkila and Winningham (1971), and Winningham (1972) on the clefts in the dayside magnetosphere. In these papers the latitude-local time extent of the cleft and its dependence on K_p were presented. In later papers Heikkila et al. (1972) and Winningham et al. (1973a) related dayside optical emissions to the causative electron and proton precipitation through the magnetospheric clefts. Further Yasuhara et al. (1973) correlated latitudinal changes in the cleft with AE

and interplanetary B_Z. The present study does not imply by omission a lack of correlation between the equatorward boundaries of stiz and particle precipitation at local times other than those encompassed by the low-altitude cleft (8-16 hours magnetic local time). Indeed evidence for correlation does exist (Winningham et al., 1973b) at other local times. However studies of the particle data at other local times is at a more rudimentary stage and a complete local time survey of the stiz particle precipitation relationship will await these studies.

The relationship between cleft particle precipitation and stiz has been investigated by studying simultaneous sounder and particle measurements obtained by ISIS-1 in the period 2-11 February, 1969. Suitable data were obtained on forty passes covering local magnetic times of 0800 to 1400. The cleft coincides with the auroral oval in the daytime sector (Heikkila et al., 1972; Winningham et al., 1973a) so that if the stiz is directly associated with auroral phenomena, coincidence might be expected between the stiz and the cleft particle precipitation. To test this the location of the stiz equatorward boundary has been plotted against the cleft equatorward boundary (Fig. 6). If the two are coincident the points will lie between the two dashed lines which indicate the errors in the measurements. Many points do indicate coincidence but a significant number indicate that the stiz can begin equatorward of the cleft. There is no indication that the stiz ever begins poleward of the cleft.

In the previous discussion the cleft equatorward boundary was defined as the onset of electron and proton fluxes with spectra similar to those observed in the magnetosheath. In addition, in the morning hours the cleft equatorward boundary is marked by the poleward cessation of > 1 kev electron fluxes. At times $\lesssim$300 eV electrons (but no low energy protons) appear at sub-cleft latitudes, i.e. on closed magnetic field lines. Figure 7 illustrates two different electron latitudinal profiles. In the Figure 7a

$\lesssim$300 eV electron precipitation commences in the cleft, whereas in Figure 7b it begins equatorward. If the stiz equatorward boundary is plotted against the equatorward boundary of $\lesssim$ 300 eV electron precipitation rather than the cleft boundary, then much better agreement is obtained (Figure 8). Note, however, that the cleft and $\lesssim$300 eV boundaries are equivalent in two thirds of the cases.

A similar comparison between the stiz and the equatorward boundary of $\gtrsim$300 eV electron precipitation revealed no definite correlation. In fact no stiz-particle correlation could be found anywhere within a region of $\gtrsim$300 eV precipitation.

In the $\lesssim$ 300 eV comparisons shown in Figure 8 there are only four anomalous cases and these have been examined in more detail. For three of these cases the 300 eV electron flux began equatorward of the stiz but was quite weak and produced no significant increase in the total particle flux. In fact good agreement is found between the stiz and cleft equatorward boundaries for these cases as indicated by the vertical arrows in Figure 8. This implies that although the stiz is related to $\lesssim$300 eV electron precipitation, the precipitation must reach some threshold value before the stiz occurs. It is planned to pursue this point further.

In the remaining anomalous case the stiz occurred equatorward of the $\lesssim$300 eV electron precipitation. These data were obtained at about 1630 UT on 10 February, 1969. Explorer 33 satellite measurements indicate that there were several reversals of the interplanetary magnetic field on that day from 1100 UT onwards. The location of particle precipitation can alter drastically under such conditions (Burch, 1972; Yasuhara et al., 1973). If the particle precipitation moves to a different location the stiz will remain at the

old location until the irregularities decay under the action of normal ionospheric processes. It seems likely that this is the explanation for the case in question and this is further supported by the fact that the severity of the spread F increased markedly near the cleft boundary (see horizontal arrow in Figure 8).

A similar procedure was adopted in studying the poleward boundaries of the stiz and particle precipitation. However coincidences between the stiz poleward boundary and those of the cleft and $\lesssim$300 eV electron precipitation were not very common. The stiz nearly always extended poleward of the particle precipitation.

Discussion

The result of the previous section show that the equatorward boundary of the stiz and of the $\lesssim$ 300 eV electron precipitation are correlated but that the correlation between the poleward boundaries is unclear. Three anomalous cases in the study of the equatorward boundary indicate that the particle spectrometer can detect $\lesssim$300 eV electron fluxes weaker than necessary for the occurrence of spread F. Therefore the disagreement of the poleward boundaries cannot be attributed to a lack of sensitivity in the particle measurements. If we interpret the agreement between the equatorward boundaries as indicating that the irregularities are produced in the region of particle precipitation the disagreement of the poleward boundaries can be explained by the drift of irregularities towards the pole as a result of magnetospheric convection (Axford and Hines, 1961; Cauffman & Gurnett, 1971).

The agreement between $\lesssim$300 eV particle precipitation and the stiz suggests that there is a causal relationship. Precipitating $\lesssim$300 eV

electrons produce most of their ionization in the F_2 region (Rees, 1964) so that spatial and temporal variations in the particle flux will produce irregularities in electron concentration. Similarly there will be variations in the heating of the ionosphere by the particle precipitation and these will also give rise to irregularity in the electron concentration, particularly at high altitudes. Variations in electron temperature near the F_2 peak result in changes in the scale height of the ionosphere so that even quite small temperature variations at this level can cause large electron concentration variations at higher altitudes (say 1000 km and above). Such a process must be important if particle precipitation produces the stiz since the stiz occurs at altitudes as high as 3000 km. Of course, other processes which may occur in conjunction with the precipitation could also produce irregularities.

The results of Dyson et al. (1973), showing that the irregularity amplitude increases with scale size, were interpreted as indicating that energy was fed into the irregularities at the larger scale sizes and that this energy was dissipated by generating smaller irregularities as in turbulence. The ionizing and heating effects of precipitating particles discussed above could produce irregularities with horizontal dimensions of at least tens of kilometres if such variations were present in the precipitating flux and so are consistent with these ideas. The irregularities would be expected to exist below the F_2 peak and what we have termed the stiz is probably the topside counterpart of the "fliz" (F layer irregularity zone) in the bottomside ionosphere reported by Pike (1971, 1972).

Conclusion

Within the spread F region at high latitudes a zone of very severe irregularities (stiz) occurs. The equatorward boundary of the stiz is quite abrupt and is consequently an efficient reflector of HF radio waves.

On the dayside of the earth, the equatorward boundary of the stiz coincides with the equatorward edge of $\lesssim$300 eV electron precipitation. Very often this $\lesssim$300 eV boundary is at the boundary of the cleft. The stiz extends poleward of the $\lesssim$300 eV precipitation probably because magnetospheric convection moves the irregularities poleward of the region of production. The correlation between the stiz and the precipitation supports the idea that the irregularities result from the precipitation. The ionizing and heating effects of the precipitating electrons will produce irregularities but other processes occurring in association with the precipitation may also contribute to the production of irregularities.

ACKNOWLEDGEMENTS

This work was supported by Air Force Cambridge Research Laboratories Contract F196-28-72-C-0230 and NASA contracts NAS 5-11011 and NAS 5-23184. Both of the authors wish to thank W. B. Hanson and W. J. Heikkila for helpful discussions.

One of us (P.L.D.) is grateful to La Trobe University for study leave. We thank L. H. Brace of Goddard Space Flight Center for access to the Langmuir probe data.

REFERENCES

Axford, W. I. and C. O. Hines, A unifying theory of high-latitude geophysical phenomena and geomagnetic storms, Can. J. Phys., 39, 1433, 1961.

Burch, J. T., Precipitation of low-energy electrons at high latitudes: effects of interplanetary magnetic field and dipole tilt angle, J. Geophys. Res., 71, 6696, 1972.

Calvert, W. and C. W. Schmid, Spread F observations by the Alouette topside sounder datellite, J. Geophys. Res., 69, 1839, 1964.

Cauffman, D. P. and D. A. Gurnett, Double-probe measurements of convection electric fields with Injun-5 satellite, J. Geophys. Res., 76, 6014, 1971.

Dyson, P. L., Topside spread F as midlatitudes, J. Geophys. Res., 73, 2441, 1968.

Dyson, P. L., Direct measurements of the size and amplitude of irregularities in the topside ionosphere, J. Geophys. Res., 74, 6291, 1969.

Dyson, P. L., On the significance of electrostatic probe observations of electron density irregularities, J. Geophys. Res., 76, 4689, 1971.

Dyson, P. L., J. P. McClure and W. B. Hanson, In-situ measurements of amplitude and scale size characteristics of ionospheric irregularities, (submitted to J. Geophys. Res. 1973).

Florida, C. D., The development of a series of ionospheric satellites, Proc. IEEE, 57, 867, 1969.

Heikkila, W. J., J. B. Smith, J. Tarstrup and J. D. Winningham, The soft particle spectrometer in the ISIS 1 satellite, Rev. Sci. Instrum., 41, 1393, 1970.

Heikkila, W. J., and J. D. Winningham, Penetration of magnetosheath plasma to low altitudes through the dayside magnetospheric cusps, J. Geophys. Res., 76, 883, 1971.

Heikkila, W. J., J. D. Winningham, R. H. Eather and S. I. Akasofu, Auroral emissions and particle precipitation in the noon sector, J. Geophys. Res., 77, 4100, 1972.

Hice, J. D. and B. Frank, Occurrence patterns of topside spread F on Alouette ionograms, J. Geophys. Res., 71, 3653, 1966.

Petrie, L. E., Preliminary results on mid and high latitude topside spread F, Spread F and Its Effect upon Radiowave Propagation and Communication, Technivision, England, p. 67, 1966.

Pike, C. P., A latitudinal survey of the daytime polar F layer, J. Geophys. Res., 76, 7745, 1971.

Pike, C. P., Equatorward shift of the polar F layer irregularity zone as a function of the Kp index, J. Geophys. Res., 77, 6911, 1972.

Rees, M. H., Note on the penetration of energetic electrons into the earth's atmosphere, Planet. Space Sci., 12, 722, 1964.

Winningham, J. D., Penetration of magnetosheath plasma to low altitudes through the dayside magnetospheric cusps, Dissertation, Texas A&M University, 1970.

Winningham, J. D., Characteristics of magnetosheath plasma observed at low altitudes in the dayside magnetospheric cusps, in Earth's Magnetospheric Processes, edited by B. M. McCormac, D. Reidel, Dordrecht, Netherlands, 1972.

Winningham, J. D., S.-I. Akasofu, F. Yasuhara and W. J. Heikkila, Simultaneous observations of auroras from the south pole station and of precipitating electrons by ISIS-1, (to be published in J. Geophys. Res.) 1973a.

Winningham, J. D., C. D. Anger, P. L. Dyson, G. G. Shepherd, and J. H. Whitteker, Correlated ISIS-2 observations of the diffuse aurora, to be submitted to J. Geophys. Res., 1973.

Yasuhara, F., S.-I. Akasofu, J. D. Winningham, and W. J. Heikkila, The equatorward shift of the cleft during magnetospheric substorms as observed by ISIS-1, submitted to J. Geophys. Res., 1973.

FIGURE CAPTIONS

Figure 1. Consecutive ISIS-2 ionograms obtained on December 9, 1971 showing onset of severe spread F at satellite height

(a) 0558:10UT Λ = 77.0°, MLT = 13.3 hours, severe spread F at satellite height,

(b) 0557:41UT Λ = 75.8°, MLT = 13.2 hours, no severe spread F at satellite height.

Figure 2. ISIS-2 ionograms exhibiting (a) short range echo and (b) long range echo.

Figure 3. Ray paths giving rise to echoes when the satellite is equatorward of the stiz region. As well as the vertical incidence echo (v), two additional echoes occur, one at a shorter range (s) and the other at a longer range (l) than the vertical incidence echo.

Figure 4. The virtual range at 2 MHz of short and long range echoes as a function of the time before (after) the satellite crossed the stiz boundary when travelling poleward (equatorward). The dotted line corresponds to a range change at the total satellite velocity (ISIS-2 is in a 1400 km circular orbit).

Figure 5. Comparison of the stiz (a) with the irregularity absolute amplitude (b) and percentage amplitude (c). ISIS-2 measurements obtained on December 9, 1971. The stiz has been characterized by the frequency spread at the satellite height (Δf_{scat}). The sensitivity of the irregularity amplitude measurements is 2.5% of the background electron concentration.

Figure 6. Comparison of the equatorward boundaries of cleft precipitation and stiz based on ISIS-1 data.

Figure 7. Examples of electron spectrograms from ISIS-1:

(a) well defined cleft (no equatorward precipitation)

(b) 300 eV electron precipitation equatorward of cleft precipitation.

Figure 8. Comparison of the equatorward boundaries of 300 eV electron precipitation and stiz based on ISIS-1 data. Arrows indicate position of cleft boundary.

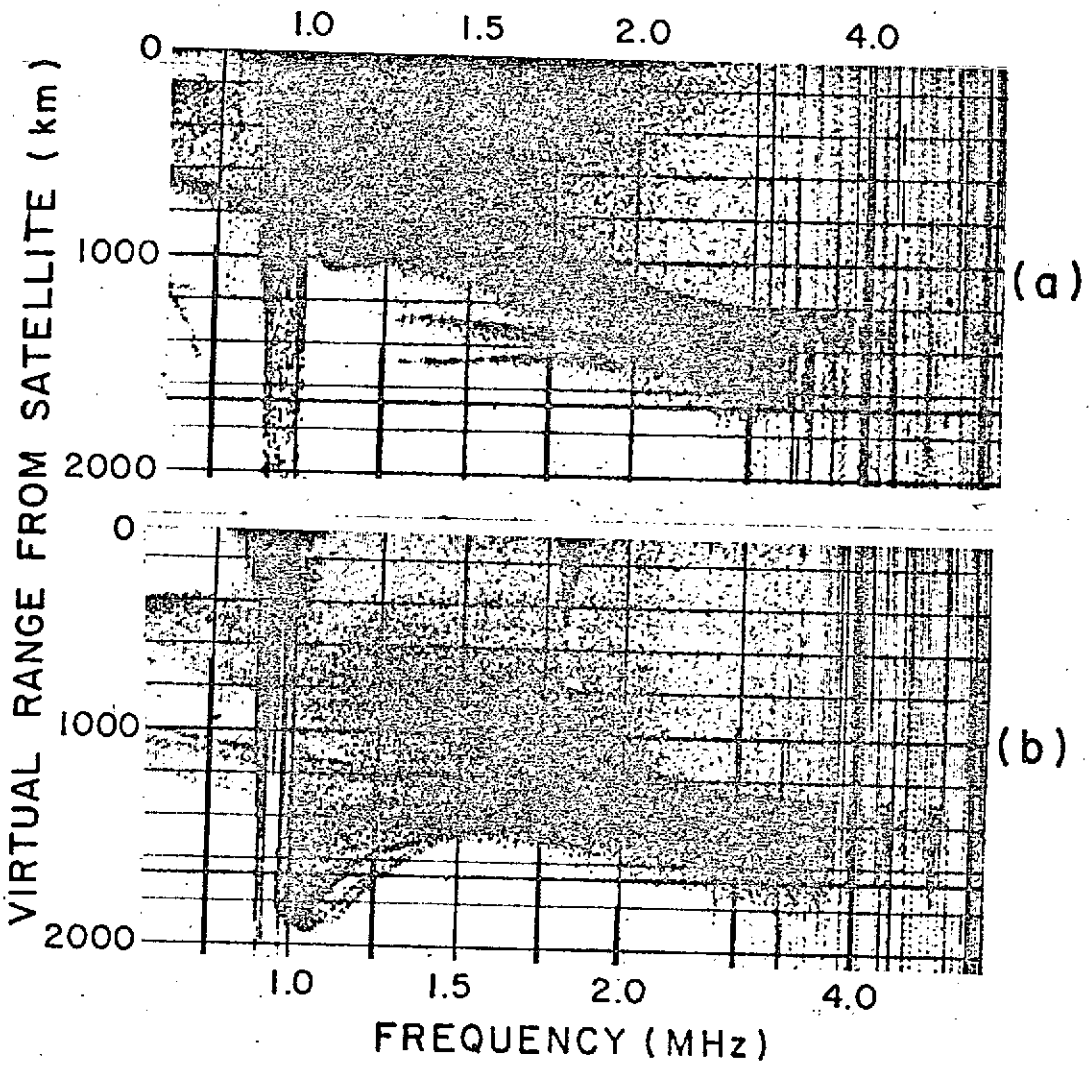
1.0
1.5
2.0
4.0
0
1000
2000
VIRTUAL RANGE FROM SATELLITE (km)
(a)
(b)
FREQUENCY (MHz)

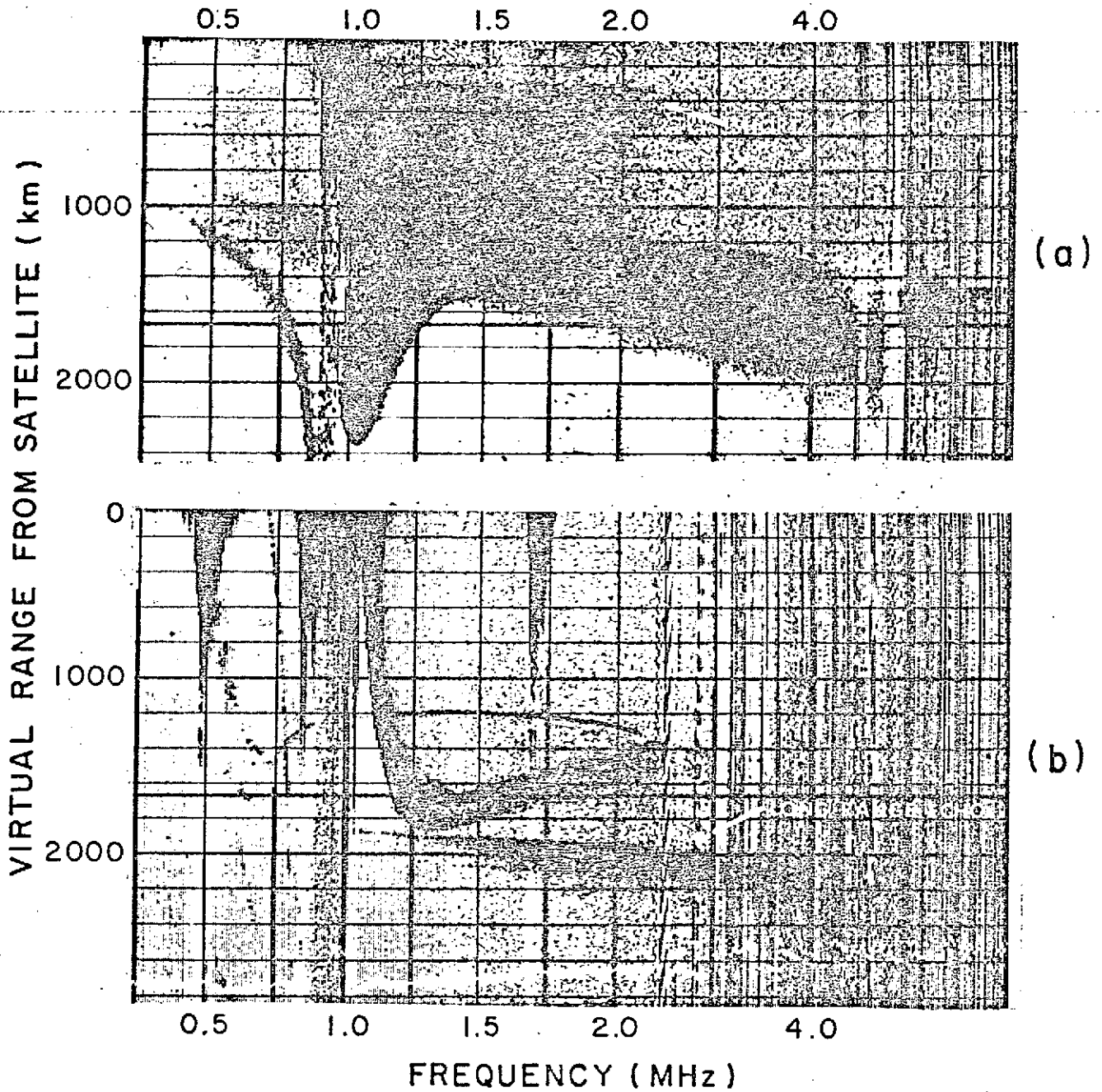
0.5
1.0
1.5
2.0
4.0
1000
2000
(a)
0
1000
2000
(b)
VIRTUAL RANGE FROM SATELLITE (km)
0.5
1.0
1.5
2.0
4.0
FREQUENCY (MHz)

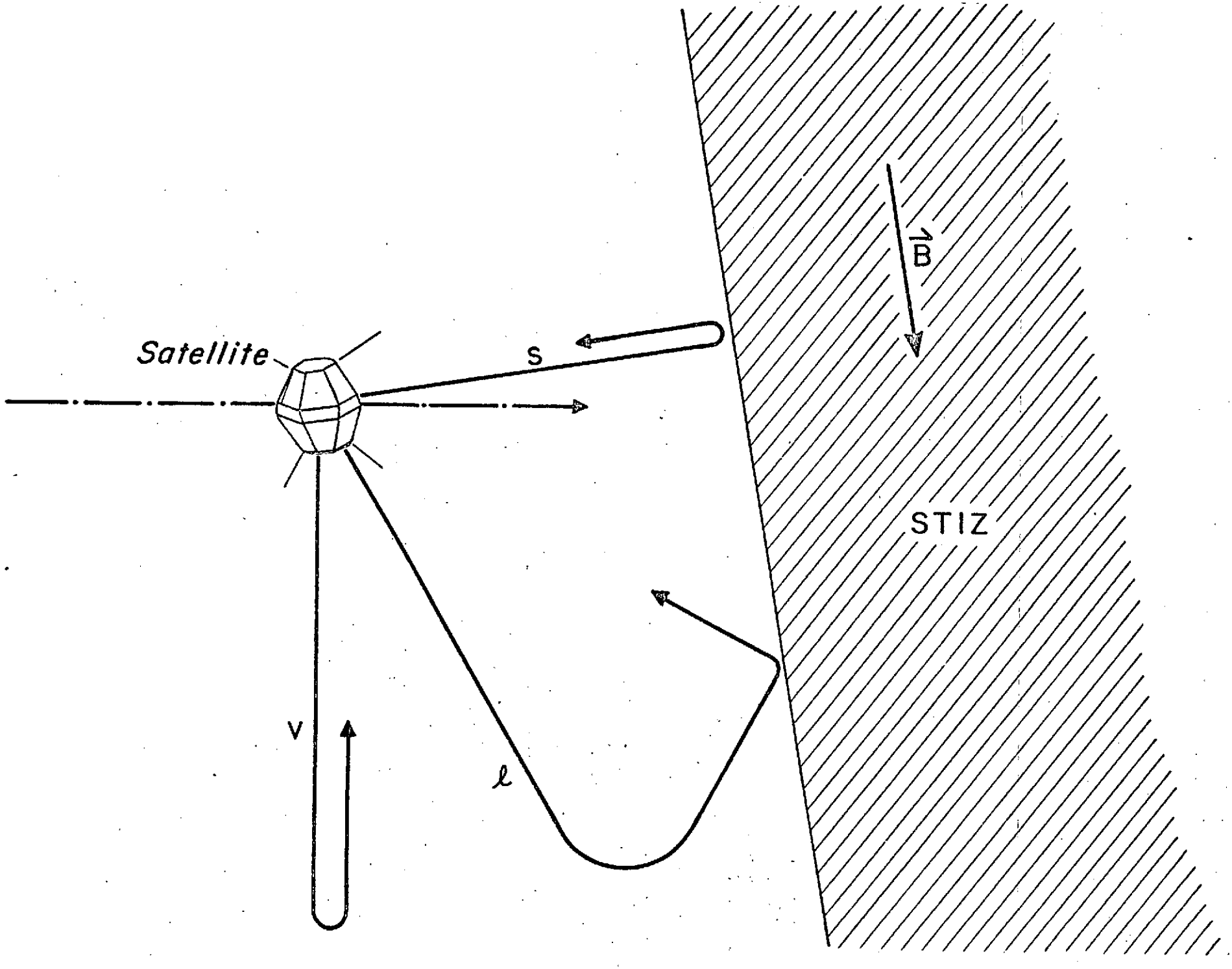
Satellite
S
$\vec{B}$
STIZ
V
ℓ

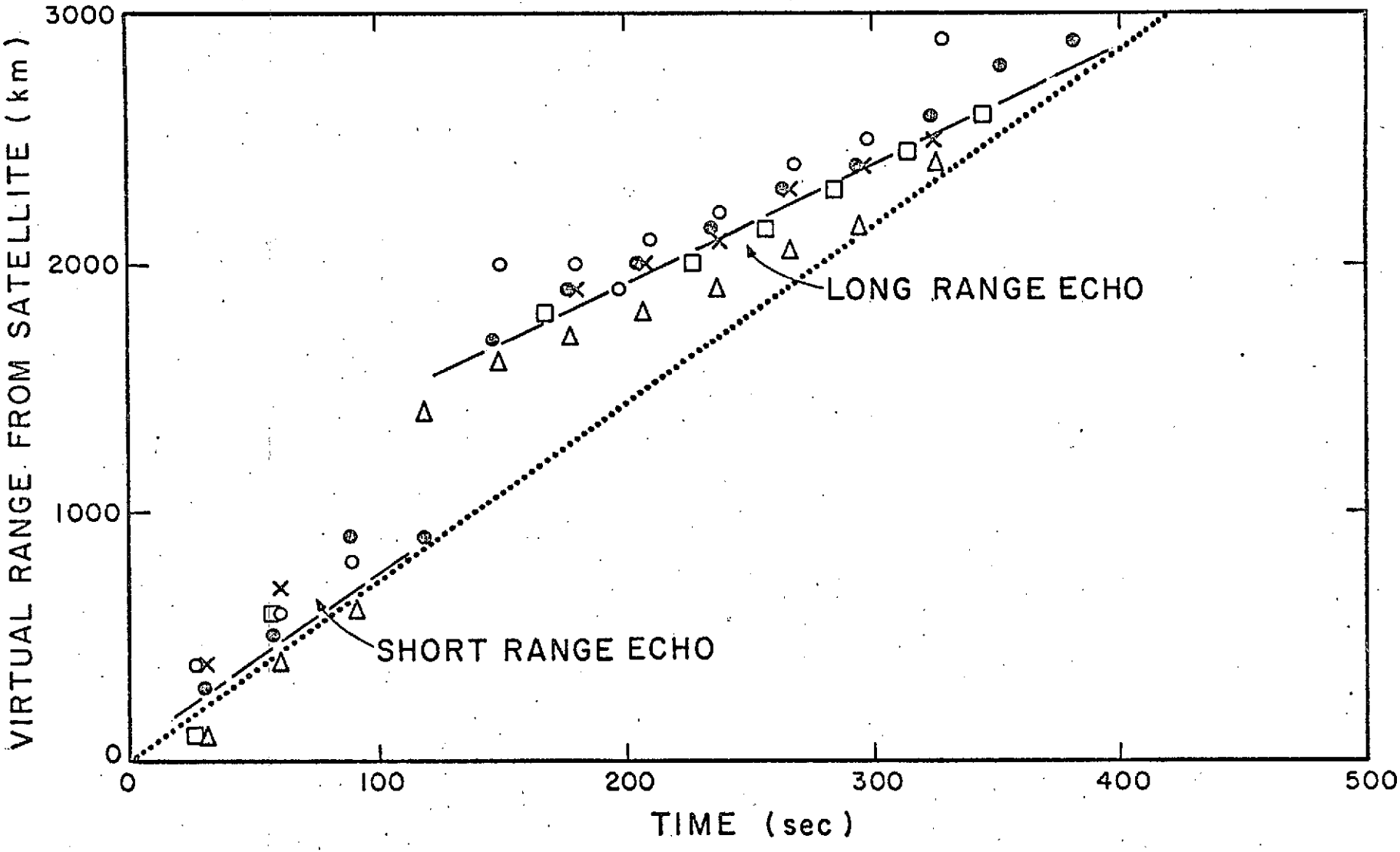
VIRTUAL RANGE FROM SATELLITE (km)
3000
2000
1000
0
0
100
200
300
400
500
TIME (sec)
LONG RANGE ECHO
SHORT RANGE ECHO

FIG 4

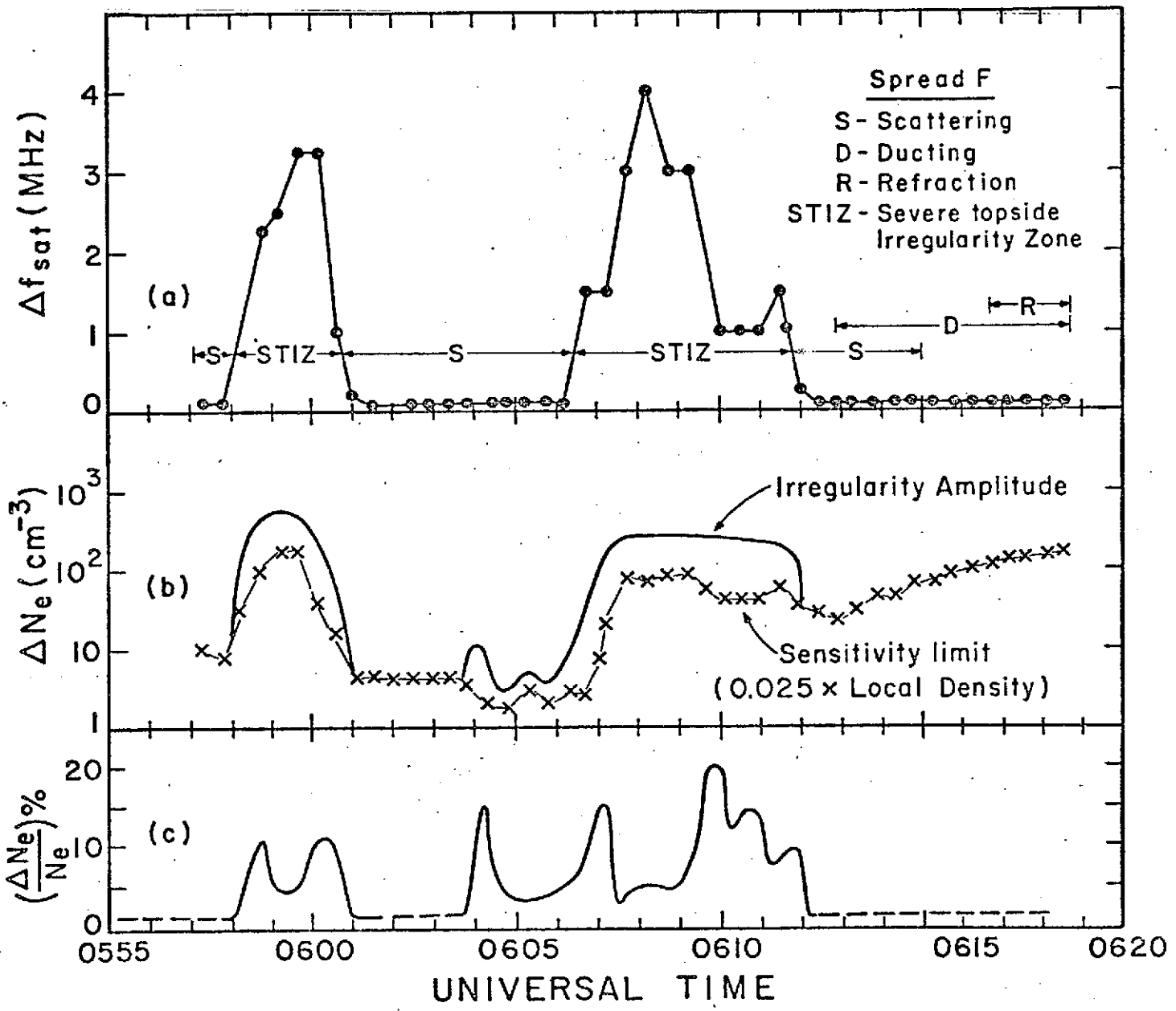
Spread F
S - Scattering
D - Ducting
R - Refraction
STIZ - Severe topside Irregularity Zone
(a)
S
STIZ
S
STIZ
S
D
R
Δf_{sat} (MHz)
(b)
Irregularity Amplitude
Sensitivity limit
(0.025 × Local Density)
ΔN_e (cm^{-3})
(c)
$\left(\frac{\Delta N_e}{N_e}\right)$%
0555
0600
0605
0610
0615
0620
UNIVERSAL TIME

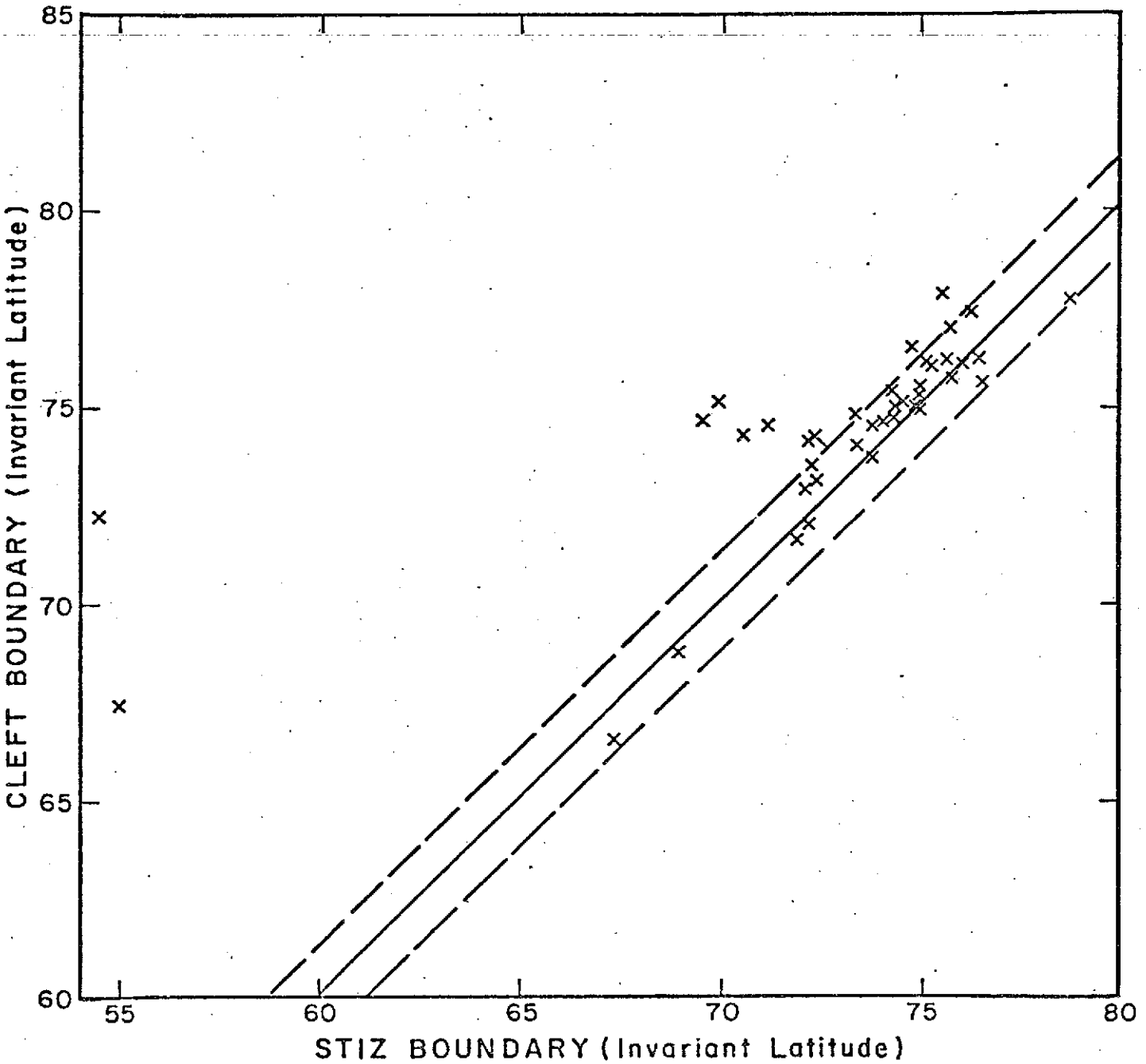
85
80
75
70
65
60
55
60
65
70
75
80
CLEFT BOUNDARY (Invariant Latitude)
STIZ BOUNDARY (Invariant Latitude)

81.5 80.1 78.5 76.9 75.3 73.7 72.0 70.4 68.8 67.2 65.6 64.0 62.4 60.9 59.4 57.9
RADIAL ENERGY
EV
4
3
2
1
TOTAL NUMBER FLUX
/CM(2) STER SEC
10
9
8
7
6
TOTAL ENERGY FLUX
ERG / CM(2) STER SEC
1
0
-1
-2
-3
-4
39 40 41 42 43 44 45 46 47 48 49 50 51 52 53 54
UNIVERSAL TIME
037/23/38/04 09/39/01LT
DATE PROCESSED: 70/10/12
TAPE NO. 9037BD
ORBIT NO. 86
LATITUDE = -73
LONGITUDE = 154
ALTITUDE = 2894
ETA = 0.7
LATITUDE = -38
LONGITUDE = 154
ALTITUDE = 3484

7a

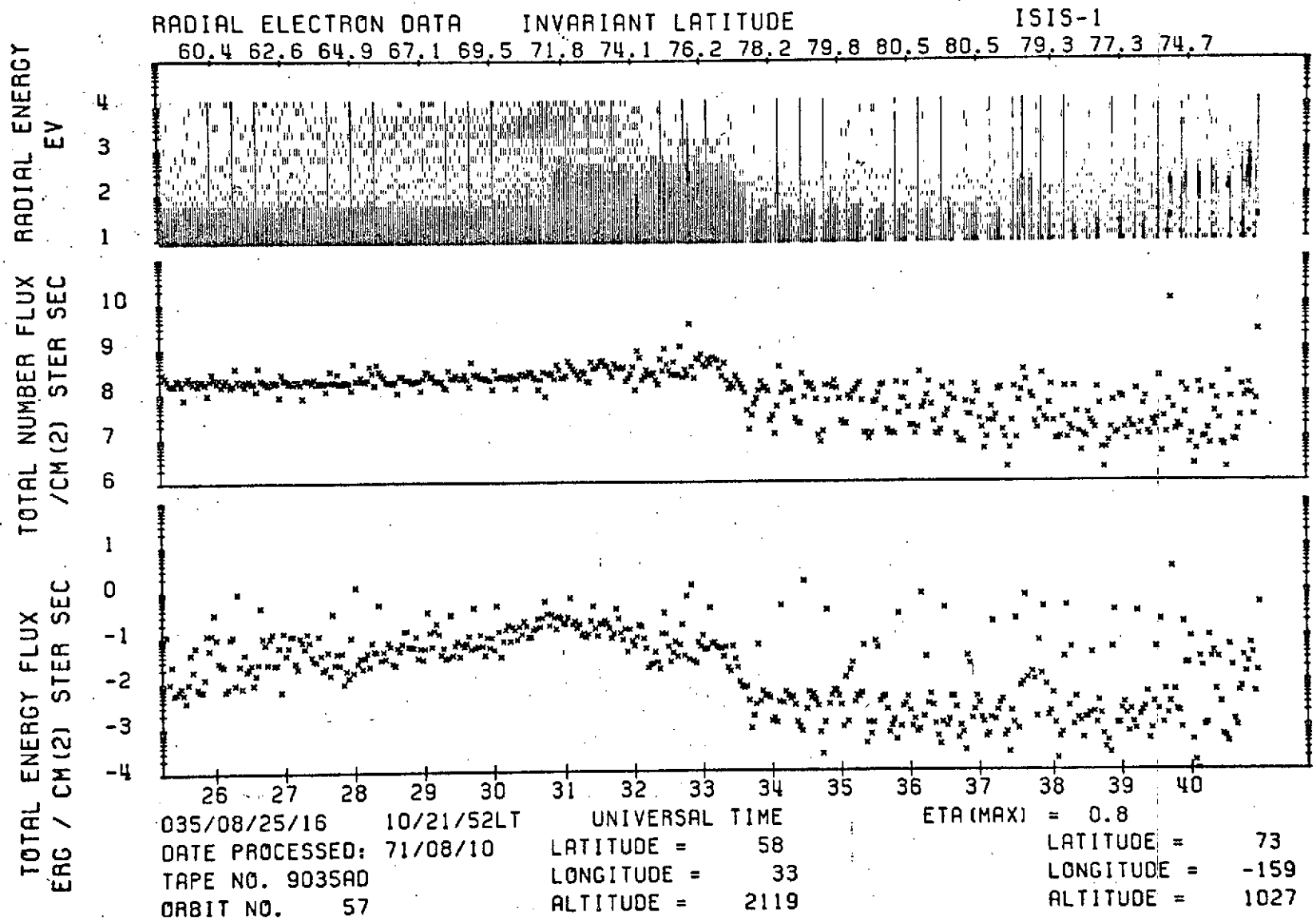
RADIAL ELECTRON DATA
INVARIANT LATITUDE
ISIS-1
60.4 62.6 64.9 67.1 69.5 71.8 74.1 76.2 78.2 79.8 80.5 80.5 79.3 77.3 74.7
RADIAL ENERGY EV
TOTAL NUMBER FLUX /CM(2) STER SEC
TOTAL ENERGY FLUX ERG / CM(2) STER SEC
4
3
2
1
10
9
8
7
6
1
0
-1
-2
-3
-4
26 27 28 29 30 31 32 33 34 35 36 37 38 39 40
035/08/25/16 10/21/52LT
UNIVERSAL TIME
ETA(MAX) = 0.8
DATE PROCESSED: 71/08/10
LATITUDE = 58
LONGITUDE = 33
ALTITUDE = 2119
LATITUDE = 73
LONGITUDE = -159
ALTITUDE = 1027
TAPE NO. 9035AD
ORBIT NO. 57

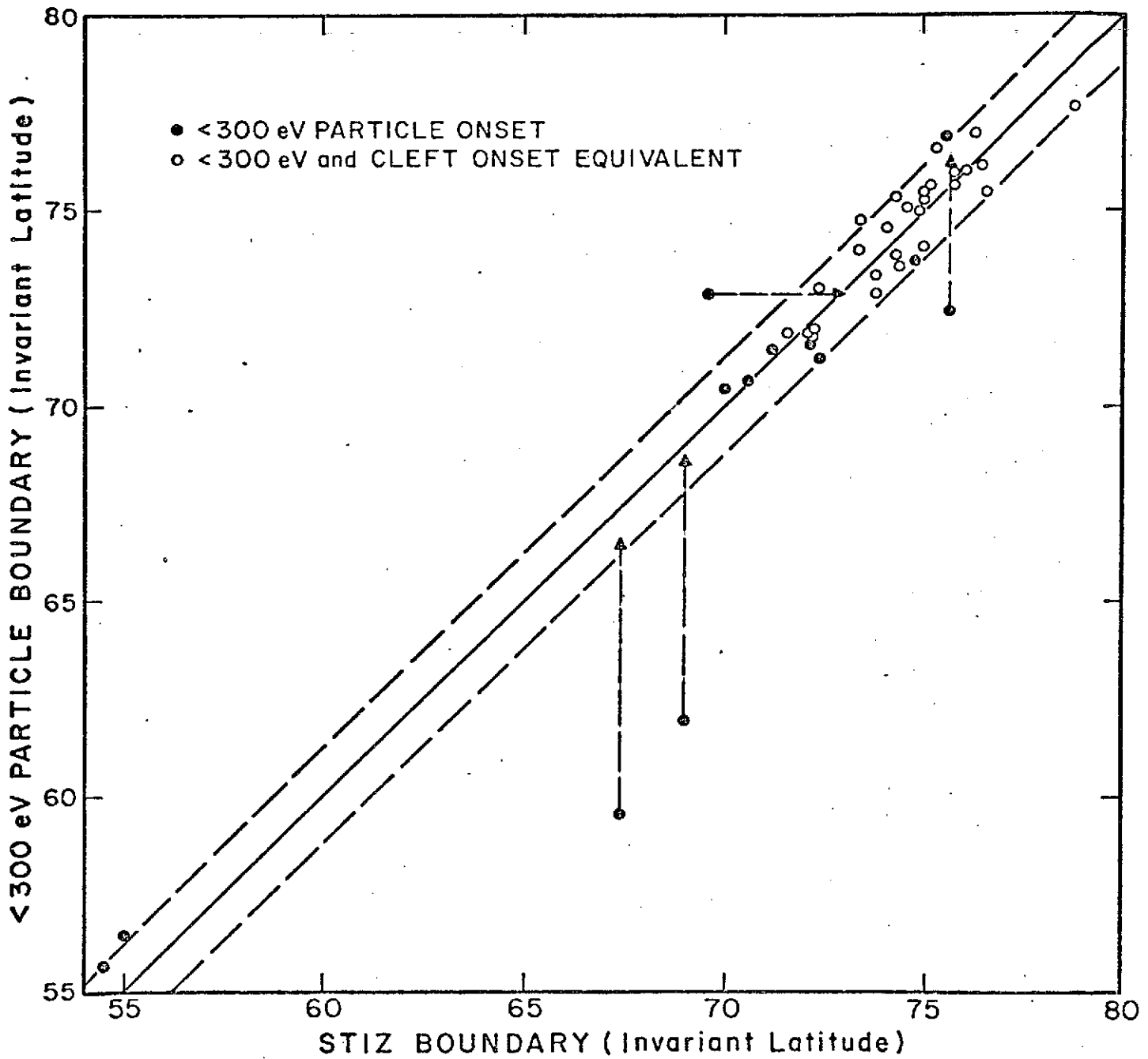
● < 300 eV PARTICLE ONSET
○ < 300 eV and CLEFT ONSET EQUIVALENT
< 300 eV PARTICLE BOUNDARY (Invariant Latitude)
STIZ BOUNDARY (Invariant Latitude)
80
75
70
65
60
55
55
60
65
70
75
80